

# Structure-Based Design, Synthesis, and Biological Evaluation of New Triazolo[1,5-*a*]Pyrimidine Derivatives as Highly Potent and Orally Active ABCB1 Modulators

Shuai Wang,<sup>†</sup> Sai-Qi Wang,<sup>†</sup> Qiu-Xu Teng,<sup>†</sup> Linlin Yang,<sup>†</sup> Zi-Ning Lei, Xiao-Han Yuan, Jun-Feng Huo, Xiao-Bing Chen, Mengru Wang, Bin Yu,\* Zhe-Sheng Chen,\* and Hong-Min Liu\*



Cite This: <https://dx.doi.org/10.1021/acs.jmedchem.0c01741>



Read Online

ACCESS |



Metrics & More

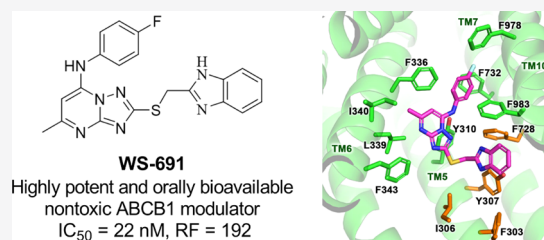


Article Recommendations



Supporting Information

**ABSTRACT:** ABCB1 is a promising therapeutic target for overcoming multidrug resistance (MDR). In this work, we reported the structure-based design of triazolo[1,5-*a*]pyrimidines as new ABCB1 modulators, of which **WS-691** significantly increased sensitization of ABCB1-overexpressed SW620/Ad300 cells to paclitaxel (PTX) ( $IC_{50} = 22.02$  nM). Mechanistic studies indicated that **WS-691** significantly increased the intracellular concentration of PTX and [<sup>3</sup>H]-PTX while decreasing the efflux of [<sup>3</sup>H]-PTX in SW620/Ad300 cells by inhibiting the efflux function of ABCB1. The cellular thermal shift assay suggested that **WS-691** could stabilize ABCB1 by directly binding to ABCB1. **WS-691** could stimulate the activity of ABCB1 ATPase but had almost no inhibitory activity against CYP3A4. Importantly, **WS-691** increased the sensitivity of SW620/Ad300 cells to PTX *in vivo* without observed toxicity. Collectively, **WS-691** is a highly potent and orally active ABCB1 modulator capable of overcoming MDR. The triazolo[1,5-*a*]pyrimidine may be a promising scaffold for developing more potent ABCB1 modulators.



## INTRODUCTION

Multidrug resistance (MDR) is one of the major reasons for the failure of successful cancer chemotherapy.<sup>1</sup> Initially, cancer patients can respond to drug treatment, while most of them develop resistance to targeted chemotherapy during treatment.<sup>2</sup> Although there are many underlying mechanisms of MDR, the predominant one is the increased efflux of drugs mediated by the upregulation of ATP-binding Cassette (ABC) transporters.<sup>3–8</sup> The most well-studied and best-characterized drug transporter is ABCB1 (also known as P-glycoprotein or MDR1), as a member of ABC superfamily, which is responsible for increasing the efflux of chemotherapeutic drugs and decreasing the concentration of intracellular drugs.

ABCB1 is ubiquitously overexpressed in many MDR cancer cells,<sup>9–12</sup> making ABCB1 a promising therapeutic target to overcome MDR.<sup>13</sup> To date, numerous ABCB1 modulators have been identified<sup>5,8</sup> and can be generally divided into three generations (Figure 1A–C). As shown in Figure 1A, the first-generation ABCB1 modulators, such as verapamil and trifluoperazine,<sup>14,15</sup> had deficiencies such as serious toxicity, low therapeutic response, *etc.*<sup>16–19</sup> Relative to the first-generation ABCB1 modulators, the second-generation ABCB1 modulators, including dexverapamil and bircodar citrate (Figure 1B), showed improved potency, specificity, and lower toxicity.<sup>20–22</sup> However, these ABCB1 modulators could inhibit the activity of the drug-metabolizing enzyme CYP3A4 and thus cause unfavorable drug–drug interactions.<sup>23–25</sup> The issues hampered further development of the second-generation

ABCB1 modulators. The third-generation ABCB1 modulators, including tariquidar, zosuquidar, laniquidar, and elacridar in the clinical trials (Figure 1C), could bind to ABCB1 with high affinity and exhibit almost no pharmacokinetic interaction with other drugs.<sup>8</sup> Although some of the third-generation ABCB1 modulators (Figure 1C) have advanced into clinical trials, none of them has been approved for clinical use.<sup>12,26–29</sup> Thus, the development of nontoxic and highly efficacious ABCB1 modulators has been highly pursued for clinical application.

Our group has also been devoted to the development of novel ABCB1 modulators, and some representative compounds are shown in Figure 1D.<sup>30–32</sup> In this work, we reported the discovery of the initial hit compound **WS-36** (compound 5) from our in-house diverse compound library,<sup>33–39</sup> which was cellularly engaged to ABCB1 and increased the sensitivity of ABCB1-overexpressed SW620/Ad300 cells to PTX. Based on the binding mode of compound **WS-36**, we performed the structure-based design of triazolo[1,5-*a*]pyrimidine derivatives as new ABCB1 modulators, leading to the discovery of **WS-691**, which was well characterized as a nontoxic, highly potent,

Received: October 5, 2020

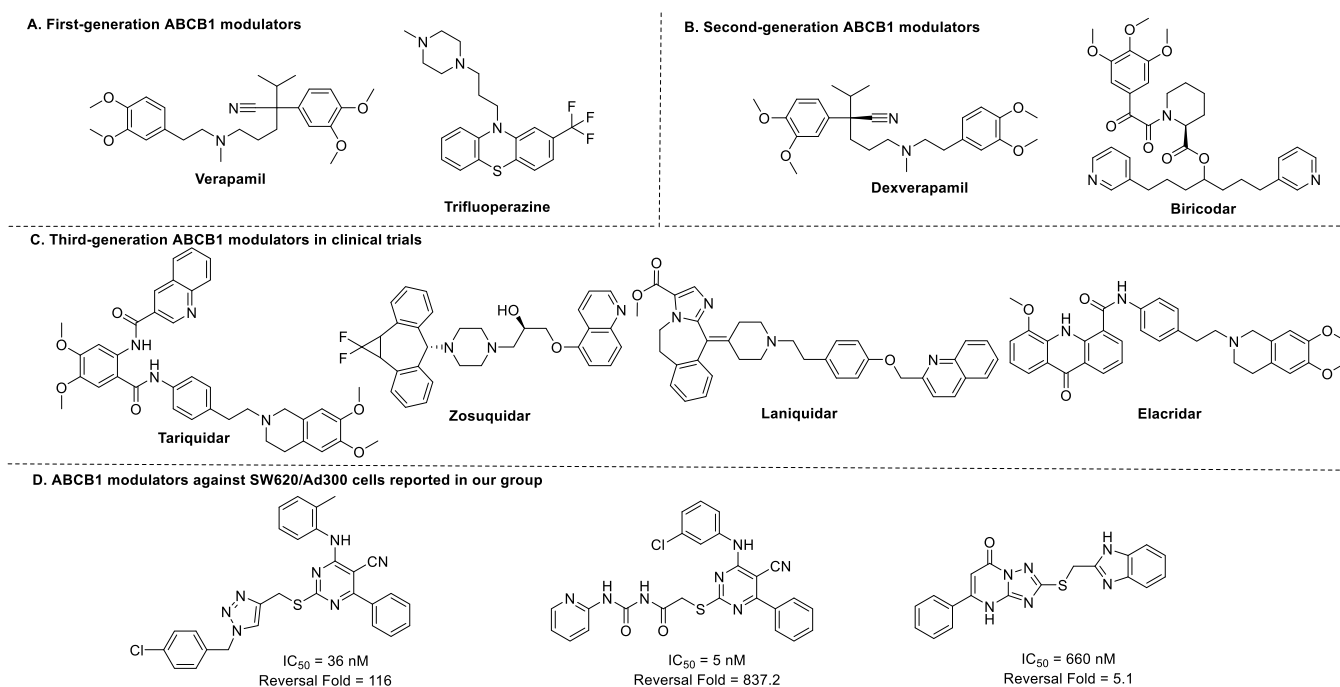
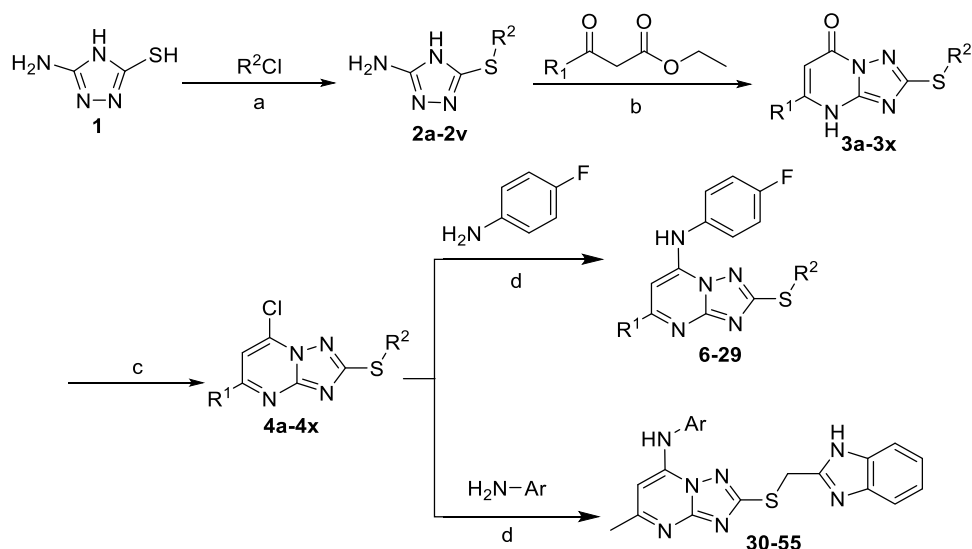


Figure 1. Some representative ABCB1 modulators.

### Scheme 1. Synthesis of Compounds 6–55<sup>a</sup>



<sup>a</sup>Reagents and Conditions: (a)  $\text{Na}_2\text{CO}_3$ , NaI, Acetone, 3–5 h, reflux; (b) acetic acid, 2–15 h, reflux; (c)  $\text{POCl}_3$ , 3–5 h, reflux; (d) EtOH, room temperature (RT), 5 h.

and orally active ABCB1 modulator capable of overcoming MDR.

## CHEMISTRY

A novel series of triazolo[1,5-*a*]pyrimidine-based derivatives targeting ABCB1 were designed and synthesized. As shown in Scheme 1, compounds 2a–2v were obtained by reacting 5-amino-4H-1,2,4-triazole-3-thiol (1) with various alkyl halides, followed by cyclization with different  $\beta$ -ketoesters, affording compounds 3a–3x. Treatment of compounds 3a–3x with  $\text{POCl}_3$  under reflux gave compounds 4a–4x, which then reacted with various amines in EtOH at room temperature to give compounds 6–55.

## RESULTS AND DISCUSSION

**Structure-Based Design of Triazolo[1,5-*a*]Pyrimidine Derivatives as New ABCB1 Inhibitors.** To identify novel and nontoxic ABCB1 inhibitors, we detected the  $IC_{50}$  values of PTX against multidrug-resistant SW620/Ad300 cells in the presence or absence of tested compounds. The cytotoxicity of tested compounds against SW620/Ad300 cells was examined, and the nontoxic concentrations (cell survival rate >90%, Table S1 in the Supporting Information) were used for examining their ability to reverse multidrug resistance. After screening our in-house library, we successfully identified the hit compound WS-36 (Figure 2A), which was nontoxic at 20  $\mu\text{M}$  (93.25% of cell survival rate) and increased the sensitivity of

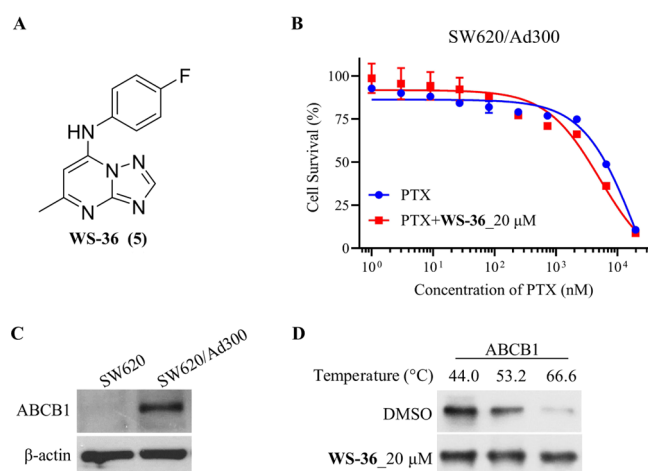


**Figure 2.** (A) Structure of WS-36. (B) *In vitro* antiproliferative activity of PTX alone or in combination with WS-36 against SW620/Ad300 cells. (C) Protein levels of ABCB1 in SW620 and SW620/Ad300 cells, and  $\beta$ -actin was used as a loading control. (D) Effect of WS-36 on the thermostability of ABCB1.

SW620/Ad300 cells to PTX (Figure 2B). When combined with WS-36 (20  $\mu$ M), PTX inhibited the cell survival of SW620/Ad300 cells with an  $IC_{50}$  value of 2.34  $\mu$ M, lower than that (4.23  $\mu$ M) when PTX was used alone. As shown in Figure 2C, compared to parental SW620 cells, ABCB1 was up-regulated in SW620/Ad300 cells. The cellular thermal shift assay (CETSA) suggested that WS-36 could bind to ABCB1 and lead to the stabilization of ABCB1 (Figure 2D).

Given the binding property of WS-36 against ABCB1, we docked it to a homology modeled human ABCB1, which was established based on the apo form of mouse ABCB1 in the inward-open conformation (PDB code: 4Q9H).<sup>40</sup> The top-scoring pose of WS-36 is bound to a central hydrophobic cavity formed by aromatic and hydrophobic residues in TMS, TM6, TM7, and TM10 (Figure 3A). A hydrogen bond was predicted between the NH of WS-36 and the benzene hydroxyl of Y310, and an edge-to-face  $\pi$ - $\pi$  stacking interaction was found between the phenyl ring of WS-36 and F983 (Figure 3B). Additionally, WS-36 was stabilized through hydrophobic contacts with the side chains of F978, F732, F336, L339, I340, and F343.

Further analysis showed that WS-36 only occupied a subpocket, leaving a large hydrophobic space (shown in a dashed red ellipse) near the triazole ring (Figure 3C), while the fluorophenyl ring in WS-36 was located in a narrow cavity (Figure 3D). The binding model of WS-36 not only rationalized its inhibitory potency against ABCB1 but also provided a structural basis for further structural optimization. Based on this binding mode, we speculate that the attachment of hydrophobic groups to the triazole ring could increase the potency of WS-36 by forming extensive interactions with the nonpolar residues in the pocket. Besides, structural modifications at the methyl group and the phenyl ring may also influence the inhibitory activity of the compounds against ABCB1. Thus, we designed the triazolo[1,5-*a*]pyrimidine-based ABCB1 inhibitors (Figure 3E).

**Structure–Activity Relationship Studies.** Based on the binding mode of WS-36 within human ABCB1, structural modifications were mainly focused on variations of substituents around the triazolo[1,5-*a*]pyrimidine scaffold. Initially, we evaluated the cytotoxicity of compounds 5–55 against PTX-

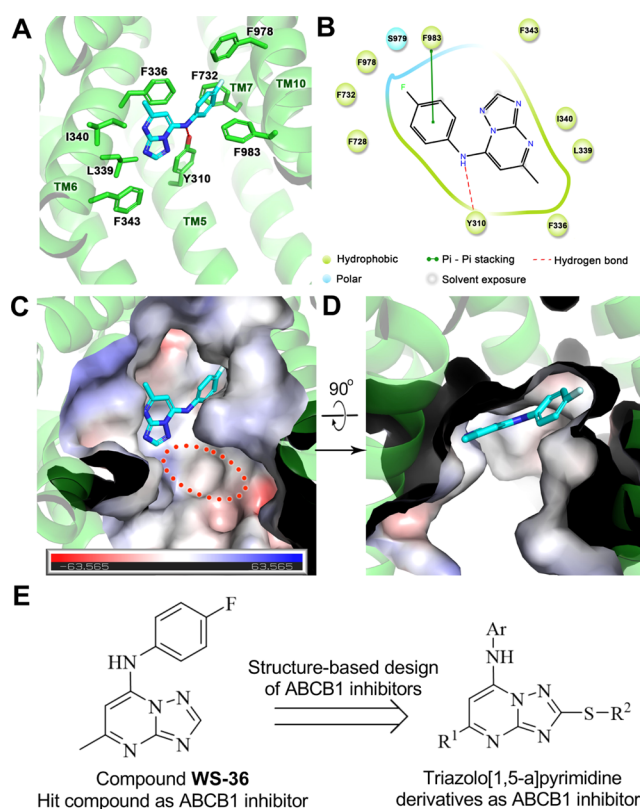


**Figure 3.** Initial evaluation of WS-36 as the ABCB1 inhibitor and further structure-based design. (A) Three-dimensional (3D)-view of interactions between WS-36 (cyan) and ABCB1 (green, PDB code: 4Q9H). The transporter is shown as a cartoon. Residues involved in interactions with WS-36 are depicted in sticks. The hydrogen bond is shown as red dashed lines. (B) Two-dimensional (2D)-view of interactions between WS-36 and ABCB1. (C) WS-36 (cyan) binds into a subpocket of a large hydrophobic cavity, the large space near the triazole is marked with red dashed lines. The electrostatic surface of this cavity is generated by PyMOL. The PyMOL charge-smoothed potential bar is shown at the bottom of this panel. (D) Fluorophenyl ring of WS-36 was located in a narrow cavity. (E) Structure-based design of new triazolo[1,5-*a*]pyrimidine-based ABCB1 inhibitors from WS-36.

resistant SW620/Ad300. The nontoxic concentrations of the compounds (a survival rate above 90% toward SW620/Ad300, provided in Table S1 in the Supporting Information) were used for the following assays. Besides, RF, representative of the reversal fold of MDR modulators based on the  $IC_{50}$  values of PTX and PTX/modulator combination, was chosen as a parameter for measuring the reversal ability of modulators. All compounds at nontoxic concentrations in combination with PTX were used to explore their effects on the reversal activity in PTX-resistant SW620/Ad300 cells, taking the well-characterized MDR modulator verapamil (VPM) as a positive control. The results are summarized in Tables 1 and 2. As shown in Table 1, PTX exhibited cytotoxicity against SW620/Ad300 cells with an  $IC_{50}$  value of 4.23  $\mu$ M, while PTX, together with VPM (4  $\mu$ M), exhibited improved cytotoxicity toward SW620/Ad300 cells with an  $IC_{50}$  value of 0.30  $\mu$ M, further confirming that VPM could reverse PTX resistance against SW620/Ad300 cells (RF = 13.90). Similarly, compounds 5–55 were evaluated to examine their reversal activity toward the SW620/Ad300 cells.

Table 1. Reversal Activity of Compounds 6–29 toward the PTX-Resistant SW620/Ad300 Cells

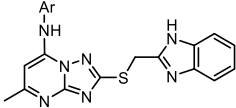
Compounds 6–29

Compound	R <sup>1</sup>	R <sup>2</sup>	IC <sub>50</sub> , PTX (μM)	RF	Compound	R <sup>1</sup>	R <sup>2</sup>	IC <sub>50</sub> , PTX (μM)	RF
PTX	--	--	4.23 ± 0.60	1.00	17	-Me		1.93 ± 0.13	2.19
VPM	--	--	0.30 ± 0.05	13.97	18	-Me		2.04 ± 0.13	2.07
6	-Me		1.04 ± 0.09	4.05	19	-Me		1.93 ± 0.08	2.19
7			1.61 ± 0.13	2.63	20	-Me		1.74 ± 0.09	2.43
8			1.44 ± 0.38	2.94	21	-Me		1.55 ± 0.06	2.73
9	-Me		1.27 ± 0.09	3.34	22	-Me		4.22 ± 0.22	1.00
10	-Me		1.89 ± 0.30	2.25	23	-Me		3.54 ± 0.13	1.19
11	-Me		1.37 ± 0.15	3.09	24	-Me		4.20 ± 0.39	1.01
12	-Me		1.64 ± 0.08	2.58	25	-Me		3.36 ± 0.26	1.26
13	-Me		2.04 ± 0.19	2.07	26	-Me		4.11 ± 0.23	1.02
14	-Me		2.57 ± 0.12	1.65	WS-691 (27)	-Me		0.022 ± 0.005	192.25
15	-Me		2.28 ± 0.08	1.86	28	-Me		2.84 ± 0.13	1.49
16	-Me		1.99 ± 0.12	2.13	29	-Me		1.26 ± 0.12	3.37

As shown in Table 1, compared to WS-36 (IC<sub>50</sub> = 2.34 μM, RF = 1.88), compound 6 bearing an additional benzylthioether group showed improved reversal activity (IC<sub>50</sub> = 1.04 μM, RF = 4.05). The data suggest that the introduction of the benzylthioether group is beneficial for the reversal activity.<sup>41</sup> Replacement of the methyl group with larger ethyl and isopropyl groups led to compounds 7 and 8, which exhibited slightly decreased reversal activity with the IC<sub>50</sub> values of 1.61 and 1.44 μM, respectively, indicating that the methyl group was favorable for the reversal activity. Therefore, subsequent modifications focused on variations of substituents attached to the phenyl ring of the benzylthioether group (R<sup>2</sup>), affording compounds 9–19, which showed comparable or decreased reversal activity with the IC<sub>50</sub> values around 2.0 μM. The results suggest that the position and electronic nature of substituents on the phenyl ring of R<sup>2</sup> have no remarkable effects on the reversal activity. Replacement of the phenyl with the naphthyl group gave compound 20, which showed comparable reversal activity against SW620/Ad300 cells (IC<sub>50</sub> = 1.74 μM, RF = 2.43). Compared with compound 6, the insertion of an additional one or two methylene spacers was proved to be detrimental for the reversal activity.

Compound 22, when combined with PTX, exhibited no reversal activity against SW620/Ad300 cells (IC<sub>50</sub> = 4.22 μM). We also found that compounds 23–26 bearing different alkyl groups failed to reverse PTX resistance against SW620/Ad300 cells. The results may suggest that the π–π and/or hydrophobic interactions with surrounding key amino acid residues within the binding pocket are crucial for the reversal activity. To further explore the structure–activity relationships (SARs), we also introduced two representative heteroaromatic groups, benzimidazole and benzothiophene, to the triazolo[1,5-*a*]pyrimidine scaffold affording compounds WS-691 (27) and 28. To our delight, WS-691 showed significantly improved reversal activity against the PTX-resistant SW620/Ad300 cells (IC<sub>50</sub> = 22.02 nM), being around 15-fold more potent than VPM (IC<sub>50</sub> = 0.30 μM). WS-691 could almost completely reverse the activity toward PTX-resistant SW620/Ad300 cells with an RF value of up to 192.25. The results suggest that the benzimidazole ring (R<sup>2</sup>) is essential for the reversal activity. Besides, compound 29 bearing the benzoyl group showed comparable or slightly increased activity against PTX-resistant SW620/Ad300 cells with compounds 6–20.

Table 2. Reversal Activity of WS-691 and Compounds 30–55 toward the PTX-Resistant SW620/Ad300 Cells



**WS-691** and compounds **30-55**

Compound	Ar	IC <sub>50</sub> , PTX (μM)	RF	Compound	Ar	IC <sub>50</sub> , PTX (μM)	RF
PTX	--	4.23 ± 0.60	1.00	<b>42</b>		4.08 ± 0.20	1.03
VPM	--	0.30 ± 0.05	13.97	<b>43</b>		0.59 ± 0.04	7.14
<b>WS-691 (27)</b>		0.022 ± 0.005	192.25	<b>44</b>		0.76 ± 0.02	5.60
<b>30</b>		0.22 ± 0.07	19.33	<b>45</b>		0.71 ± 0.05	5.99
<b>31</b>		0.52 ± 0.02	8.08	<b>46</b>		0.50 ± 0.05	8.40
<b>32</b>		0.79 ± 0.01	5.34	<b>47</b>		0.32 ± 0.04	13.18
<b>33</b>		0.77 ± 0.03	5.50	<b>48</b>		0.57 ± 0.04	7.44
<b>34</b>		0.26 ± 0.09	16.09	<b>49</b>		0.25 ± 0.05	17.27
<b>35</b>		0.47 ± 0.05	9.04	<b>50</b>		2.38 ± 0.15	1.78
<b>36</b>		0.63 ± 0.01	6.74	<b>51</b>		3.22 ± 0.23	1.31
<b>37</b>		0.85 ± 0.04	4.97	<b>52</b>		1.43 ± 0.07	3.03
<b>38</b>		0.72 ± 0.02	5.89	<b>53</b>		1.59 ± 0.19	2.67
<b>39</b>		0.046 ± 0.007	92.02	<b>54</b>		1.14 ± 0.19	3.71
<b>40</b>		0.27 ± 0.07	15.56	<b>55</b>		1.57 ± 0.33	2.70
<b>41</b>		0.45 ± 0.09	9.41				

Inspired by the potent reversal activity of **WS-691** against PTX-resistant SW620/Ad300 cells and associated with the binding mode of **WS-36** within modeled human ABCB1 (Figure 3A–C), we next modified the structures focusing on variations of substituents on the phenyl ring (Ar) of **WS-691**. As indicated in Figure 3C, the fluorophenyl ring in **WS-36** was located in a narrow cavity, and this binding mode suggests that the introduction of steric substituents or inappropriate substituent position may significantly affect the reversal activity. Initially, we explored the effect of the fluorine atom on the reversal activity. Clearly, the fluorine-containing compounds **30–38** showed significantly decreased reversal activity compared to **WS-691**, regardless of the position and the number of fluorine atoms. The results demonstrate that modifications on this phenyl ring are not well tolerated. Of note, compound **39** without any substituents on the phenyl ring also exerted promising reversal activity with an IC<sub>50</sub> of

0.046 μM (RF = 92). Similarly, the incorporation of other common substituents into the phenyl ring (compounds **40–53**) also caused a decrease of the reversal activity. These results are consistent with those observed in the fluorine-containing compounds. Notably, compounds **42**, **50**, and **51** bearing polar groups (e.g., –COOH, –OH, and amine) showed significantly decreased reversal activity against PTX-resistant SW620/Ad300 cells. Besides, compounds **54** and **55** possessing the coumarin and pyrazole ring, respectively, also exhibited decreased reversal activity. The above results suggest that steric and polar groups on the phenyl ring (Ar) may be less preferred for the reversal activity against PTX-resistant SW620/Ad300 cells.

**Effect of WS-691 on Reversing PTX Resistance.** In view of the potent reversal activity of **WS-691**, we also explored the effect of **WS-691** on the reversal of PTX resistance at different concentrations (cell survival rates under the nontoxic

Table 3. WS-691 Significantly Sensitizes SW620/Ad300 Cells to PTX

treatment	IC <sub>50</sub> of PTX (mean ± SD, nM) [reversal fold]	
	SW620	SW620/Ad300
PTX	7.69 ± 2.78 [1.00]	4233.18 ± 499.10 [1.00]
PTX + WS-691 (10 μM)	7.35 ± 2.40 [1.05]	73.60 ± 10.32 [57.52]
PTX + WS-691 (20 μM)	5.14 ± 0.95 [1.50]	22.02 ± 4.80 [192.25]
PTX + VPM (4 μM)	7.11 ± 2.88 [1.08]	303.53 ± 47.93 [13.95]

concentration of WS-691 are provided in Table S2 in the Supporting Information). As shown in Table 3, the IC<sub>50</sub> values of PTX against SW620 and SW620/Ad300 cells were 7.69 and 4233.18 nM, respectively, suggesting that SW620/Ad300 cells were highly resistant to PTX. WS-691 at 10 and 20 μM significantly enhanced the sensitivity of SW620/Ad300 cell lines to PTX, achieving about 57- and 192-fold reversal of PTX resistance, respectively. When combined with WS-691 (20 μM), PTX significantly inhibited the cell survival of SW620/Ad300 cells with an IC<sub>50</sub> value of 22.02 nM but was less potent against parental SW620 cells. The expression difference of ABCB1 in both SW620 and SW620/Ad300 cells may be responsible for the reversal effect of WS-691. VPM (4 μM) failed to increase the cytotoxicity of PTX to SW620 cells and was less potent than WS-691 in reversing MDR.

To further investigate the reversal effect of WS-691, KB-3-1 and its MDR cell line KB-C2 were used, in which KB-C2 overexpressed ABCB1 (Figure 4). As depicted in Table 4, the

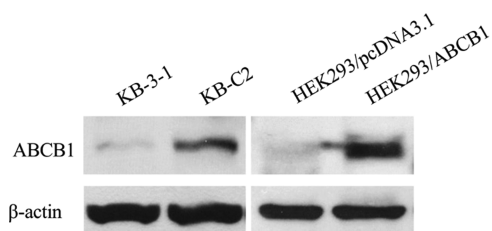


Figure 4. Protein levels of ABCB1 in KB-3-1, KB-C2, HEK293/pcDNA3.1, and HEK293/ABCB1 cell lines, and β-actin was used as the loading control.

IC<sub>50</sub> values of PTX against KB-3-1 and KB-C2 cells were 4.54 and 1886.37 nM, respectively, and the data indicated that compared to the parental KB-3-1 cells, KB-C2 cells exhibited 415.50-fold resistance to PTX. WS-691 at 10 μM effectively reversed the PTX resistance with an RF value of 86.89, and WS-691 at 20 μM totally reversed the PTX resistance of KB-C2 cells with an IC<sub>50</sub> value of 4.75 nM. Intriguingly, WS-691, in combination with PTX, showed little effect on the parental KB-3-1 cells. The results supported that the reversal effect of WS-691 may be closely related to ABCB1.

To further investigate whether the reversal effect of WS-691 was related to ABCB1, we detected the reversal effect of WS-691 against ABCB1 gene transfectant cell line HEK293/

ABCB1 (Figure 4). As shown in Table 5, the HEK293/ABCB1 cells displayed about 47-fold resistance to PTX, compared to the parental HEK293/pcDNA3.1 cells. WS-691, whether at 10 or 20 μM, showed little effect on the cytotoxicity of PTX against HEK293/pcDNA3.1 cells. However, WS-691, at 10 μM, exhibited almost the same reversal activity as VPM toward PTX-resistant HEK293/ABCB1 cells, while WS-691, at 20 μM, showed 2-fold improvement of the reversal activity, compared to VPM. WS-691, whether at 10 or 20 μM, showed almost no effect on the efficacy of PTX against the parental cell lines but could significantly reverse the resistance of ABCB1-overexpressed SW620/Ad300, KB-C2, and HEK293/ABCB1 cells to PTX. WS-691, especially at 20 μM, showed much better reversal ability than the well-known ABCB1 modulator VPM. The results strongly suggest that WS-691 reversed MDR of SW620/Ad300, KB-C2, and HEK293/ABCB1 cells to PTX by modulating ABCB1.

#### Effect of WS-691 on Accumulation and Efflux of PTX.

Given the potent reversal activity of WS-691, we next measured the intracellular concentration of PTX in SW620 and SW620/Ad300 cells by ultra-performance liquid chromatography (UPLC). As illustrated in Figure 5A, because of ABCB1-mediated drug efflux, the concentration of PTX in ABCB1-overexpressed SW620/Ad300 cells was significantly lower than that in SW620 cells without treatment. Compared to the untreated group, WS-691 significantly increased the intracellular concentration of PTX in SW620/Ad300 cells in a dose-dependent manner. After treatment with WS-691 (20 μM), the intracellular concentration of PTX in SW620/Ad300 cells was slightly higher than that in cells treated with VPM (4 μM).

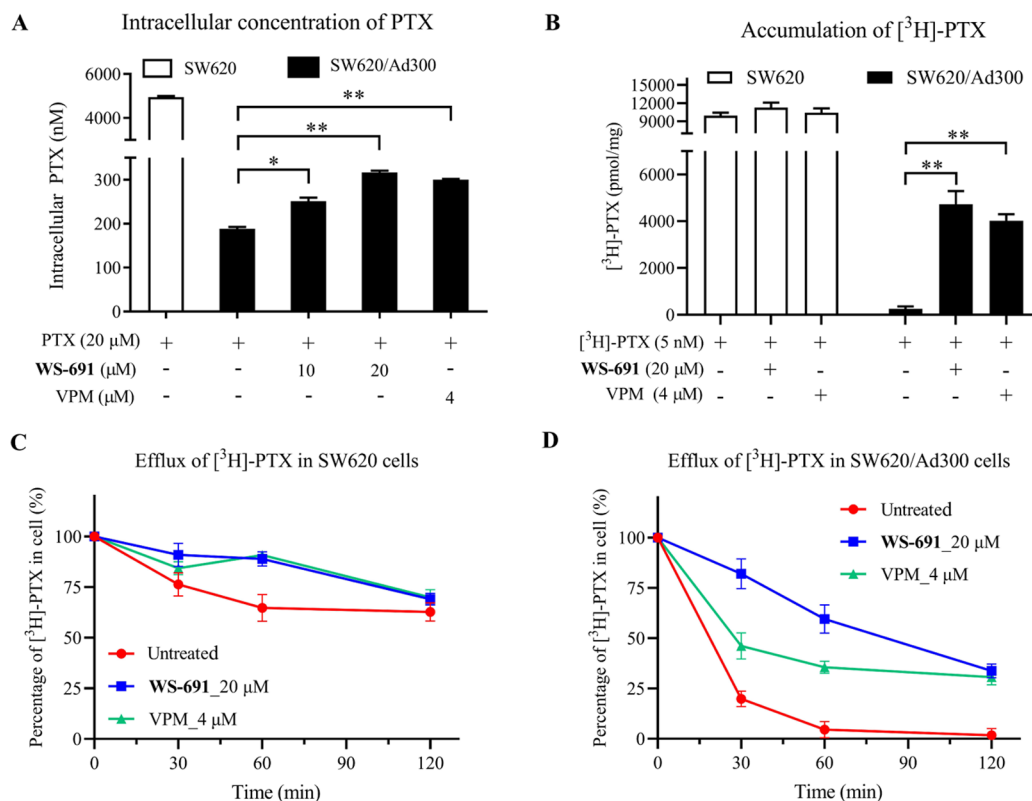
Besides, we also detected the concentration of tritium-labeled PTX ([<sup>3</sup>H]-PTX) in SW620 and SW620/Ad300 cells. As illustrated in Figure 5B, the concentration of [<sup>3</sup>H]-PTX in ABCB1-overexpressed SW620/Ad300 cells was also significantly lower than that in SW620 cells without treatment with WS-691 or VPM. Upon treatment of SW620 cells with VPM at 4 μM, the concentration of [<sup>3</sup>H]-PTX in SW620 cells was not changed obviously, while WS-691 at 20 μM also failed to increase [<sup>3</sup>H]-PTX in SW620 cells. To our delight, the concentrations of [<sup>3</sup>H]-PTX in SW620/Ad300 cells treated with WS-691 (20 μM) or VPM (4 μM) significantly increased, compared to the untreated control. The results indicate that WS-691 could increase the intracellular concentration of PTX.

Table 4. WS-691 Significantly Sensitizes KB-C2 Cells to PTX

treatment	IC <sub>50</sub> of PTX (mean ± SD, nM) [reversal fold]	
	KB-3-1	KB-C2
PTX	4.54 ± 1.59 [1.00]	1886.37 ± 243.05 [1.00]
PTX + WS-691 (10 μM)	3.95 ± 0.81 [1.15]	21.71 ± 3.27 [86.89]
PTX + WS-691 (20 μM)	2.99 ± 0.47 [1.52]	4.75 ± 1.52 [397.13]
PTX + VPM (4 μM)	3.84 ± 1.25 [1.18]	7.05 ± 2.81 [267.57]

Table 5. WS-691 Significantly Sensitizes HEK293/ABCB1 Cells to PTX

treatment	IC <sub>50</sub> of PTX (mean ± SD, nM) [reversal fold]	
	HEK293/pcDNA3.1	HEK293/ABCB1
PTX	1.93 ± 0.06 [1.00]	91.40 ± 23.32 [1.00]
PTX + WS-691 (10 μM)	1.48 ± 0.17 [1.30]	10.35 ± 4.52 [8.83]
PTX + WS-691 (20 μM)	1.50 ± 0.04 [1.29]	5.03 ± 3.27 [18.17]
PTX + VPM (4 μM)	1.62 ± 0.16 [1.19]	10.37 ± 5.47 [8.81]



**Figure 5.** Effect of WS-691 on accumulation and efflux of PTX. (A) Effect of WS-691 on the intracellular concentration of PTX in SW620 and SW620/Ad300 cells. (B) Effect of WS-691 on the accumulation of [<sup>3</sup>H]-PTX in SW620 and SW620/Ad300 cells. (C) Effect of WS-691 on the efflux of [<sup>3</sup>H]-PTX in SW620 cells. (D) Effect of WS-691 on the efflux of [<sup>3</sup>H]-PTX in SW620/Ad300 cells. Error bars represent the standard deviation (SD) value obtained from the average of three independent experiments. \*,  $P < 0.05$  and \*\*,  $P < 0.01$ .

We also found that WS-691 exhibited better potency than VPM in increasing the accumulation of PTX in SW620/Ad300 cells.

Next, we examined whether WS-691 could inhibit the efflux function of ABCB1. The effect of WS-691 on the efflux of [<sup>3</sup>H]-PTX was also explored in SW620 and SW620/Ad300 cells by monitoring the concentration of [<sup>3</sup>H]-PTX at the four different time points. As depicted in Figure 5C, the treatment of SW620 cells with WS-691 (20 μM) or VPM (4 μM) slightly decreased efflux of [<sup>3</sup>H]-PTX, compared to the untreated cells. Intriguingly, compared to the untreated group, after treatment with WS-691 (20 μM) or VPM (4 μM), the efflux of [<sup>3</sup>H]-PTX was significantly inhibited in SW620/Ad300 cells, leading to 64 and 62% loss of [<sup>3</sup>H]-PTX, respectively, in SW620/Ad300 cells after 120 min, which was obviously lower than that (97% loss) in the untreated group (Figure 5D). All of these data suggest that WS-691 could inhibit the efflux function of ABCB1, thus reducing PTX efflux and increasing the intracellular concentration of PTX.

**Effect of WS-691 on ABCB1 Expression and Subcellular Localization.** The effect of WS-691 on ABCB1

expression in SW620/Ad300 cells was investigated. As shown in Figure 6A, after treatment of SW620/Ad300 cells with WS-691 at 20 μM for 48, 72, or 96 h, respectively, the protein level of ABCB1 was not changed. As an efflux pump, localization on cytomembrane ensures its efflux function of ABCB1. In Figure 6B, treatment with WS-691 at 20 μM for 72 h did not change the subcellular localization of ABCB1 (Green) in SW620/Ad300 cells. It is believed that the inhibition of the efflux function of ABCB1 or downregulation of ABCB1 has been regarded as a potential therapeutic strategy to overcome MDR.<sup>42</sup> Therefore, these data suggest that WS-691 may reverse the ABCB1-mediated MDR by inhibiting the efflux function of ABCB1 rather than changing the expression and subcellular localization of ABCB1.

**Effect of WS-691 on the ABCB1 ATP Hydrolysis.** VPM, a simulator of ABCB1-mediated ATP hydrolysis, has been reported to stimulate the ABCB1-ATPase activity.<sup>43</sup> In view of the fact that ATP consumption could indirectly reflect the activity of ATPase as drug efflux needs the energy derived from ATP hydrolysis, we therefore assessed the effect of WS-691 on the basal activity of ABCB1 ATPase by detecting ATP

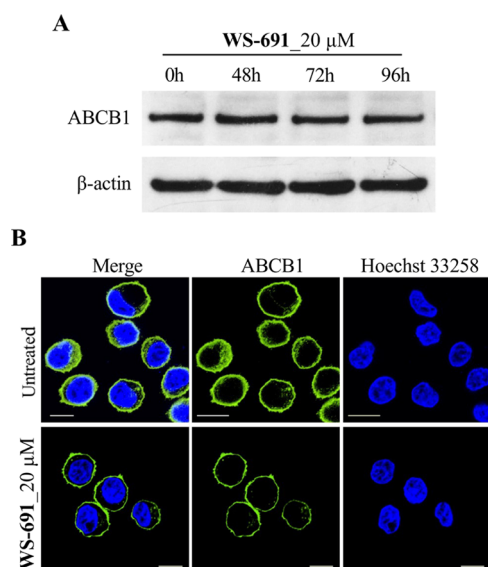


**Figure 6.** Effect of WS-691 on ABCB1 expression and subcellular localization. (A) Protein level of ABCB1 in SW620/Ad300 cells, and  $\beta$ -actin was used as a loading control. (B) Effect of WS-691 on the subcellular localization of ABCB1 (green) after treatment for 72 h. Hoechst 33342 (blue) counterstains the nuclei. The scale bar is 10  $\mu$ m.

hydrolysis in the presence of WS-691 at different concentrations (0–40  $\mu$ M). As shown in Figure 7, WS-691 stimulated ATP hydrolysis of ABCB1 to about 2.5-fold of basal activity. The ABCB1-stimulation effect of WS-691 reached maximal at a concentration of about 19.1  $\mu$ M, indicating that WS-691 could stimulate the activity of ABCB1 ATPase with a maximal value being around 2.5-fold of basal activity.

**Effect of WS-691 on Cytochrome P3A4 (CYP3A4).** The second-generation ABCB1 modulators showed better potency and specificity but with lower cell toxicity than the first-generation ABCB1 modulators. Unfortunately, these ABCB1 modulators could simultaneously inhibit the activity of the drug-metabolizing enzyme CYP3A4, which may lead to unexpected pharmacokinetic parameters and side effects.<sup>21–23,25,44</sup> Therefore, the CYP3A4 activity assay was

performed to explore the interaction between CYP3A4 and WS-691, a well-known CYP3A4 inhibitor ketoconazole and VPM were used as the positive controls. As shown in Figure 8A, compared to the solvent control, at 30  $\mu$ M, ketoconazole and VPM sharply decreased the activity of CYP3A4 in a time-dependent manner, while WS-691 displayed mild activation of CYP3A4. Besides, as shown in Figure 8B, ketoconazole and VPM showed strong and moderate inhibitory effects on CYP3A4 activity, respectively, while WS-691 displayed a very slight activation effect on CYP3A4. At 30 min, WS-691 (20  $\mu$ M) changed the activity of CYP3A4 to 1.06-fold of that at 0 min. At 37  $^{\circ}$ C, the  $IC_{50}$  values of ketoconazole and VPM were 0.011 and 21.33  $\mu$ M, respectively. These data suggested that WS-691 had almost no effect on the activity of CYP3A4, indicating possible low toxicity of WS-691 as an ABCB1 modulator.

**Cellular Thermal Shift Assay (CETSA).** ABCB1 has been reported to be the second most important ABC transporter in MDR, and most ABCB1 modulators generally exhibited inhibitory activity toward ABCB1.<sup>45</sup> Therefore, to investigate whether WS-691 could selectively bind to ABCB1 in SW620/Ad300 cells, the cellular thermal shift assay was carried out.<sup>46</sup> As shown in Figure 9, pretreatment with WS-691 significantly inhibited the degradation of ABCB1 protein caused by high temperature, compared to the solvent control. On the contrary, WS-691 showed no obvious effect on ABCB1 degradation. The data suggest that WS-691 could selectively stabilize ABCB1 by directly binding to ABCB1.

**Molecular Modeling Analysis.** Compound WS-691 was docked into the human ABCB1 model. WS-691 had a similar binding mode compared with WS-36 but formed more hydrophobic interactions with ABCB1. The fluorophenyl ring of WS-691 almost overlapped with that of WS-36, and a  $\pi$ - $\pi$  stacking interaction was also formed with F983. The triazolo[1,5-*a*]pyrimidine scaffold shifted a little from the space occupied by WS-36 and, thus, lost the hydrogen bond interaction with Y310 (Figure 10A,B). As expected, the benzimidazole ring of WS-691 extended to TM7 and TM10, forming two  $\pi$ - $\pi$  stacking interactions with F983 and F728, respectively, as well as many nonspecific contacts with Y307, I306, and F303 (Figure 10C).

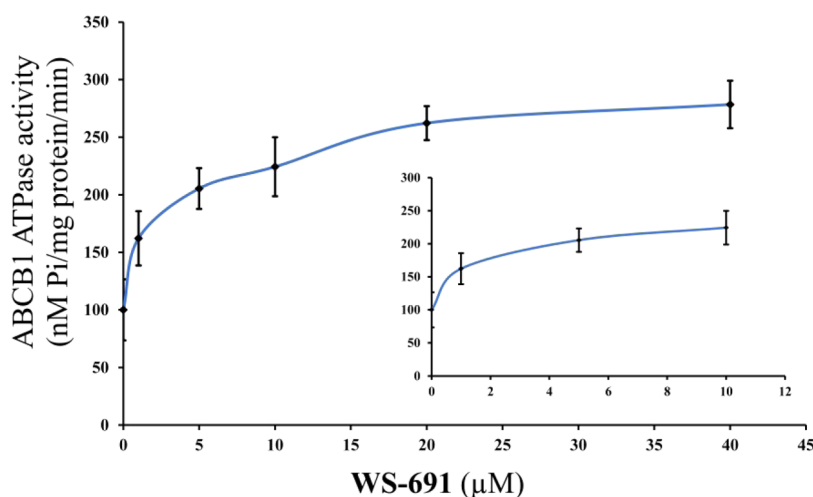


**Figure 7.** Effect of WS-691 on the ABCB1 ATP hydrolysis. The graph plotted the change of average ATPase activity of ABCB1 with SD as the concentration of WS-691 changed. The inset shows the stimulation of ATP hydrolysis at a lower concentration of WS-691.

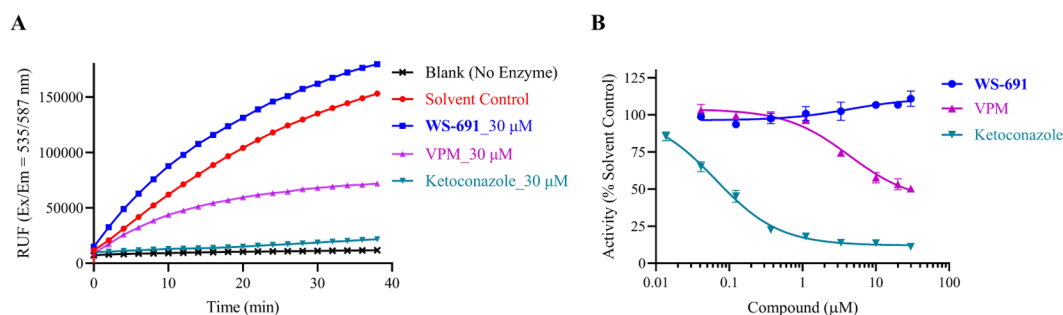


**Figure 8.** Effect of WS-691 on the activity of CYP3A4. (A) Reaction kinetics of fluorogenic substrate metabolism in human liver microsomes containing CYP3A4 at 37 °C. (B) Dose–response curve of WS-691, VPM, and ketoconazole on CYP3A4.

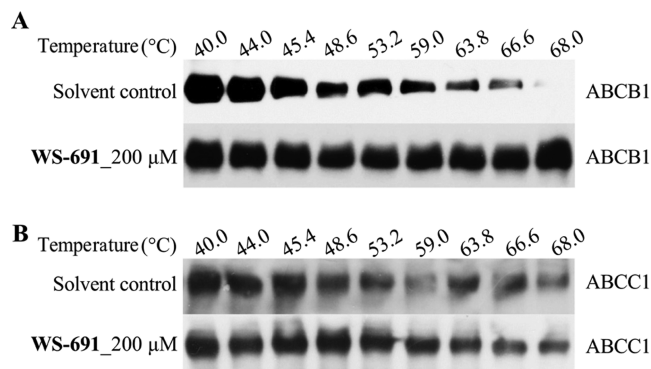


**Figure 9.** Binding of WS-691 with ABCB1. The aliquots of SW620/Ad300 cell lysate in the presence or absence of WS-691 were heated, and ABCB1 and ABCC1 were assessed by Western blotting.

**Xenograft Study.** Inspired by the encouraging *in vitro* potency of WS-691, we examined the antitumor effect of WS-691 and PTX *in vivo* using an established xenograft model bearing SW620/Ad300 cells in nude mice. Animals were treated with vehicle, PTX, WS-691, VPM, PTX plus WS-691, or PTX plus VPM, respectively. During the therapy, the tumor weight and volume were measured every 2 days. As shown in Figure 11A,B, the combination of PTX with WS-691 showed stronger antitumor activity than PTX alone. The tumor weight and volume in the group treated with PTX/WS-691 combination were smaller than that treated with PTX alone, while WS-691 showed little effect on the tumor growth compared to the vehicle group. It is remarkable that WS-691, in combination with PTX, showed superior antitumor potency

than VPM. No mortality or significant change in body weight was observed during the treatment with the tested doses (Figure 11C). The HE and TUNEL staining of tumor tissues (Figure 11E) showed that the combination of WS-691 and PTX led to more death (nuclear pyknosis, dark purple in HE staining) and apoptosis (bright green in TUNEL staining) of tumor cells compared to vehicle and single-drug treatment. The HE staining of liver tissues presented in Figure 11F showed that all treatments did not cause obvious liver injury, suggesting that the combination regimen did not result in increased toxicity. These data indicated that WS-691 increased the sensitivity of SW620/Ad300 cells to PTX *in vivo* without increasing toxicity.

## CONCLUSIONS

In this work, we reported the discovery of the hit compound WS-36 after screening our diverse small-molecule compound library, and subsequent extensive medicinal chemistry efforts generated a novel series of triazolo[1,5-*a*]pyrimidine-based ABCB1 modulators 6–55. In particular, PTX, in combination with WS-691 at 20 μM, significantly inhibited the growth of PTX-resistant SW620/Ad300 cells with an IC<sub>50</sub> value of 22.02 nM, being around 14-fold more potent than VPM (IC<sub>50</sub> = 303 nM), and the results indicated that WS-691 almost completely reversed the PTX resistance activity toward SW620/Ad300 cells with an RF value of up to 192.25. Further mechanistic studies revealed that WS-691 reversed the ABCB1-mediated MDR by inhibiting the efflux function of ABCB1 rather than downregulating ABCB1. Besides, WS-691 significantly increased the concentration of PTX and [<sup>3</sup>H]-PTX while decreasing the efflux of [<sup>3</sup>H]-PTX in SW620/Ad300 cells by

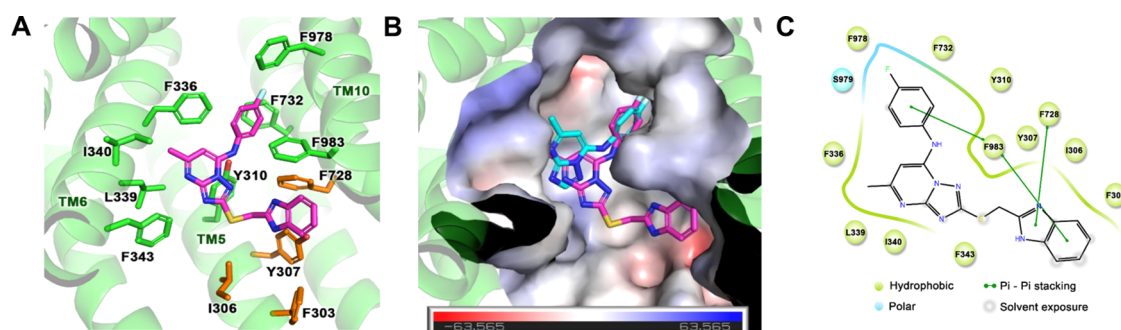


**Figure 10.** Predicted binding mode of WS-691 (PDB code: 4Q9H). (A) 3D-view of interactions between WS-691 (magenta) and ABCB1 (green). The transporter is shown as a cartoon. Residues involved in interactions with both WS-691 and WS-36 are depicted in green sticks. Residues that only interact with WS-691 are depicted in orange sticks. (B) WS-691 (magenta) binds into the same hydrophobic cavity as WS-36 (cyan) and occupies more space in the binding pocket. The electrostatic surface of this cavity is generated by PyMOL. The PyMOL Charge-smoothed potential bar is shown in the picture. (C) 2D-view of interactions between WS-691 and ABCB1.

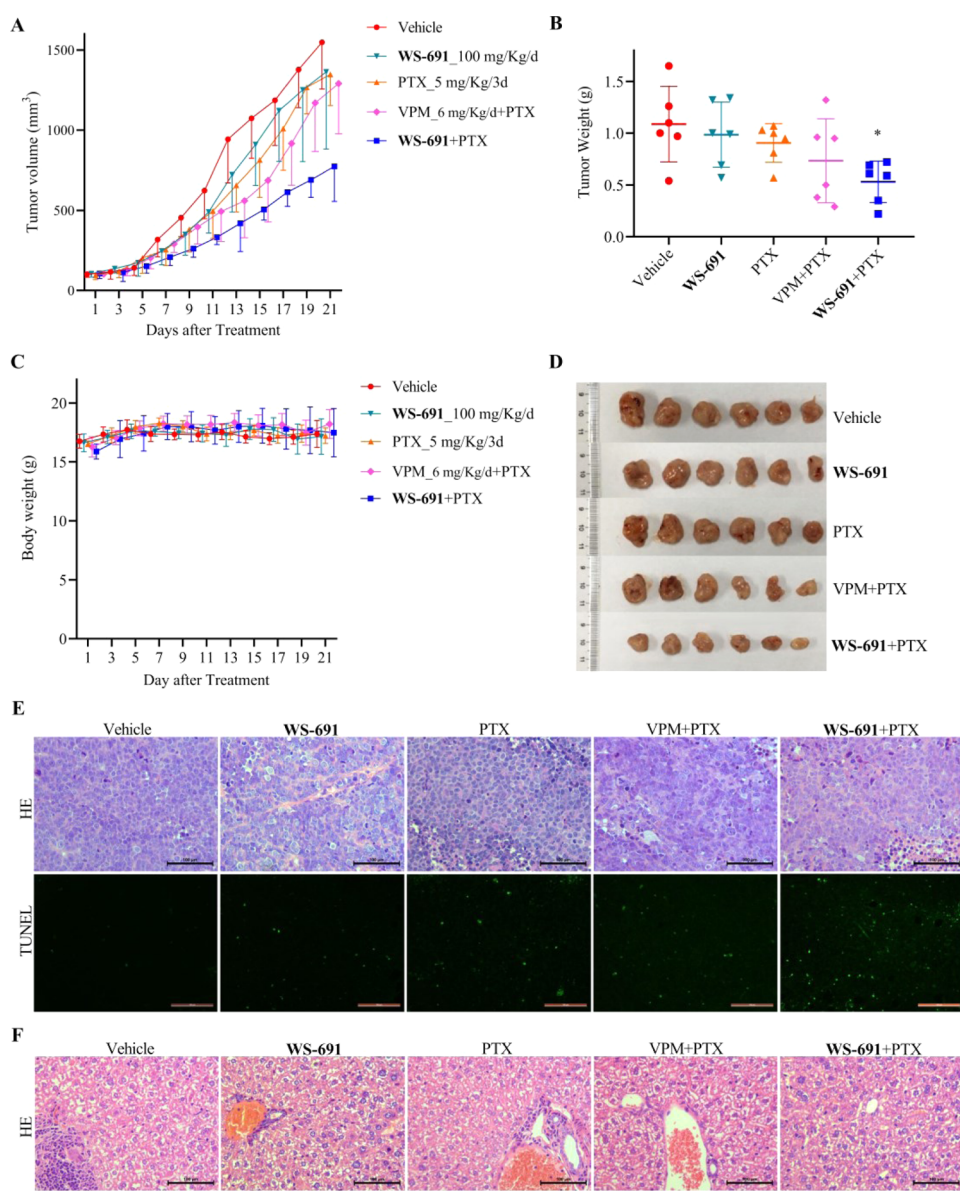


**Figure 11.** Synergistic antitumor effect of **WS-691** and **PTX** *in vivo*. (A) Tumor volume during the *in vivo* study. (B) Tumor weight at the end of the experiment. (C) Body weight of animals during the *in vivo* study. (D) Photographs of tumors at the end of the *in vivo* study. (E) HE and TUNEL staining of tumor tissues. (E) HE staining of liver tissues. The scale bar is 100  $\mu\text{m}$ . \*,  $P < 0.05$ .

inhibition of the efflux function of ABCB1. **WS-691** could stimulate the activity of ABCB1 ATPase but had almost no effect on the inhibitory activity against CYP3A4, an important enzyme of Cytochrome P450 responsible for drug metabolism in the body, and the data suggest that **WS-691** may be a safer ABCB1 modulator than VPM and Ketoconazole *in vivo* and could be synergistically used with other drugs without affecting drug–drug interactions. The cellular thermal shift assay suggested that **WS-691** could directly bind to ABCB1 and then stabilize ABCB1. More importantly, **WS-691** increased the sensitivity of SW620/Ad300 cells to PTX in a xenograft model bearing SW620/Ad300 cells without obvious toxicity. Collectively, **WS-691** is a highly effective and nontoxic ABCB1 modulator capable of overcoming multidrug resistance *in vitro* and *in vivo* and may deserve further preclinical development. The success of **WS-691** highlights the importance of the triazolo[1,5-*a*]pyrimidine scaffold for the development of new ABCB1 inhibitors.

## EXPERIMENTAL SECTION

**Chemistry.** Reagents and solvents were commercially available for direct use without further purification. A Bruker DPX 400 MHz spectrometer was used to characterize all of the NMR data and TMS in  $\text{DMSO-}d_6$  or  $\text{CDCl}_3$  selected as the internal standard. Relative to TMS,  $\delta$  ppm values were used to represent Chemical shifts. A Waters Micromass Q-T of Micromass spectrometer by electrospray ionization (ESI) was used to give high-resolution mass spectra (HRMS). Waters e2695 HPLC was used to measure the purity of compounds **5–55**, all of which were >95% pure (Phenomenex column, C-18, 5.0  $\mu\text{m}$ , 4.6 mm  $\times$  250 mm). Compounds **5–26** were detected by the acetonitrile in  $\text{H}_2\text{O}$  (40:60, v/v), and the flow rate is 1.0 mL/min, while compounds **27–41** and **43–55** were measured by acetonitrile in  $\text{H}_2\text{O}$  (55:45, v/v). Besides, compound **42** was subjected to acetonitrile in  $\text{H}_2\text{O}$  (70:30, v/v).

**General Method for the Synthesis of 4a–4x.** Compounds **4a–4x** were prepared according to the previously reported method.<sup>37</sup>

**General Method for the Synthesis of Compounds 6–55.** Compound **4a** (290.7 mg, 1 mmol) was dissolved in ethanol (2 mL), followed by the addition of commercially available 4-fluoroaniline

(111.1 mg, 1 mmol). The reaction mixture was stirred at room temperature for 5 h. Upon completion of the reaction, the solvent was evaporated, the resulting residue was then purified by column chromatography to give compound 6. Other compounds were synthesized following a similar route as described for the synthesis of compound 6.

**2-(Benzylthio)-N-(4-fluorophenyl)-5-methyl-[1,2,4]triazolo[1,5-*a*]pyrimidin-7-amine (6).** Yellow solid, yield: 92%. HPLC purity: 99.02%. m.p.: 227–231 °C. <sup>1</sup>H NMR (400 MHz, DMSO-*d*<sub>6</sub>) δ 7.52–7.45 (m, 4H), 7.36 (m, 4H), 7.29–7.23 (m, 1H), 6.37 (s, 1H), 4.57 (s, 2H), 2.45 (s, 3H). <sup>13</sup>C NMR (100 MHz, DMSO-*d*<sub>6</sub>) δ 165.20, 161.90, 160.23, 159.47, 152.44, 146.64, 137.60, 132.00, 128.95, 128.48, 127.54, 127.46, 127.36, 116.66, 116.43, 90.38, 34.58, 22.00. HRMS (ESI): *m/z* calcd for C<sub>19</sub>H<sub>15</sub>FN<sub>5</sub>S (M + H)<sup>+</sup>, 364.1032; found, 364.1040.

**2-(Benzylthio)-5-ethyl-N-(4-fluorophenyl)-[1,2,4]triazolo[1,5-*a*]pyrimidin-7-amine (7).** White solid, yield: 79%. HPLC purity: 99.56%. m.p.: 214–223 °C. <sup>1</sup>H NMR (400 MHz, DMSO-*d*<sub>6</sub>) δ 7.56–7.46 (m, 4H), 7.32 (m, 4H), 7.28–7.22 (m, 1H), 6.27 (s, 1H), 4.57 (s, 2H), 2.66 (q, *J* = 7.5 Hz, 2H), 1.19 (t, *J* = 7.5 Hz, 3H). <sup>13</sup>C NMR (100 MHz, DMSO-*d*<sub>6</sub>) δ 168.59, 164.65, 161.22, 158.80, 155.90, 145.35, 137.99, 133.01, 132.98, 128.86, 128.41, 127.19, 126.84, 126.76, 116.36, 116.14, 88.23, 34.51, 30.90, 12.85. HRMS (ESI): *m/z* calcd for C<sub>20</sub>H<sub>19</sub>FN<sub>5</sub>S (M + H)<sup>+</sup>, 380.1345; found, 380.1331.

**2-(Benzylthio)-N-(4-fluorophenyl)-5-isopropyl-[1,2,4]triazolo[1,5-*a*]pyrimidin-7-amine (8).** White solid, yield: 84%. HPLC purity: 96.35%. m.p.: 192–198 °C. <sup>1</sup>H NMR (400 MHz, DMSO-*d*<sub>6</sub>) δ 7.46 (d, *J* = 7.1 Hz, 2H), 7.33 (t, *J* = 7.1 Hz, 2H), 7.28 (d, *J* = 7.0 Hz, 1H), 6.84 (t, *J* = 8.8 Hz, 2H), 6.55 (dd, *J* = 7.7, 5.2 Hz, 2H), 5.82 (s, 1H), 4.46 (s, 2H), 2.86 (m, 1H), 1.24 (d, *J* = 6.8 Hz, 6H). <sup>13</sup>C NMR (100 MHz, DMSO-*d*<sub>6</sub>) δ 162.63, 160.21, 155.86, 155.73, 153.58, 151.88, 145.52, 137.93, 129.31, 128.95, 127.78, 115.64, 115.42, 115.16, 115.08, 95.98, 35.06, 32.12, 21.33. HRMS (ESI): *m/z* calcd for C<sub>21</sub>H<sub>21</sub>FN<sub>5</sub>S (M + H)<sup>+</sup>, 394.1502; found, 394.1487.

**2-((4-Fluorobenzyl)thio)-N-(4-fluorophenyl)-5-methyl-[1,2,4]triazolo[1,5-*a*]pyrimidin-7-amine (9).** White solid, yield: 92%. HPLC purity: 98.94%. m.p.: 184–191 °C. <sup>1</sup>H NMR (400 MHz, DMSO-*d*<sub>6</sub>) δ 7.56 (dd, *J* = 8.6, 5.6 Hz, 2H), 7.52–7.46 (m, 2H), 7.37 (dd, *J* = 12.2, 5.4 Hz, 2H), 7.15 (t, *J* = 8.9 Hz, 2H), 6.37 (s, 1H), 4.57 (s, 2H), 2.45 (s, 3H). <sup>13</sup>C NMR (100 MHz, DMSO-*d*<sub>6</sub>) δ 165.04, 162.61, 161.89, 160.19, 159.46, 152.55, 146.60, 134.07, 134.04, 132.01, 131.03, 130.95, 127.55, 127.46, 116.65, 116.42, 115.32, 115.10, 90.35, 33.69, 22.07. HRMS (ESI): *m/z* calcd for C<sub>19</sub>H<sub>16</sub>F<sub>2</sub>N<sub>5</sub>S (M + H)<sup>+</sup>, 384.1094; found, 384.1093.

**2-((4-Chlorobenzyl)thio)-N-(4-fluorophenyl)-5-methyl-[1,2,4]triazolo[1,5-*a*]pyrimidin-7-amine (10).** White solid, yield: 93%. HPLC purity: 97.76%. m.p.: 183–189 °C. <sup>1</sup>H NMR (400 MHz, DMSO-*d*<sub>6</sub>) δ 7.55 (d, *J* = 8.4 Hz, 2H), 7.49 (dd, *J* = 9.0, 4.9 Hz, 2H), 7.37 (t, *J* = 8.8 Hz, 4H), 6.36 (s, 1H), 4.56 (s, 2H), 2.45 (s, 3H). <sup>13</sup>C NMR (100 MHz, DMSO-*d*<sub>6</sub>) δ 164.89, 161.87, 160.46, 159.44, 152.64, 146.56, 137.03, 132.03, 131.92, 130.84, 128.37, 127.53, 127.45, 116.64, 116.41, 90.31, 33.71, 22.14. HRMS (ESI): *m/z* calcd for C<sub>19</sub>H<sub>16</sub>ClFN<sub>5</sub>S (M + H)<sup>+</sup>, 400.0799; found, 400.0799.

**2-((4-Bromobenzyl)thio)-N-(4-fluorophenyl)-5-methyl-[1,2,4]triazolo[1,5-*a*]pyrimidin-7-amine (11).** White solid, yield: 89%. HPLC purity: 99.94%. m.p.: 180–186 °C. <sup>1</sup>H NMR (400 MHz, DMSO-*d*<sub>6</sub>) δ 7.50 (m, 6H), 7.37 (t, *J* = 8.8 Hz, 2H), 6.37 (s, 1H), 4.54 (s, 2H), 2.45 (s, 3H). <sup>13</sup>C NMR (100 MHz, DMSO-*d*<sub>6</sub>) δ 164.91, 161.90, 160.28, 159.47, 152.42, 146.63, 137.43, 131.97, 131.29, 131.20, 127.56, 127.48, 120.45, 116.65, 116.42, 90.39, 33.77, 22.00. HRMS (ESI): *m/z* calcd for C<sub>19</sub>H<sub>16</sub>BrFN<sub>5</sub>S (M + H)<sup>+</sup>, 444.0294; found, 444.0276.

**2-((2-Bromobenzyl)thio)-N-(4-fluorophenyl)-5-methyl-[1,2,4]triazolo[1,5-*a*]pyrimidin-7-amine (12).** White solid, yield: 85%. HPLC purity: 99.08%. m.p.: 174–181 °C. <sup>1</sup>H NMR (400 MHz, DMSO-*d*<sub>6</sub>) δ 7.76–7.63 (m, 2H), 7.48 (dd, *J* = 8.9, 5.0 Hz, 2H), 7.40–7.30 (m, 3H), 7.24 (m, 1H), 6.26 (s, 1H), 4.64 (s, 2H), 2.39 (s, 3H). <sup>13</sup>C NMR (100 MHz, DMSO-*d*<sub>6</sub>) δ 164.16, 163.81, 158.92, 155.57, 145.38, 136.85, 132.88, 132.73, 131.41, 129.61, 127.92, 127.08, 126.99, 124.50, 124.02, 116.42, 116.19, 89.33, 35.27, 24.48.

HRMS (ESI): *m/z* calcd for C<sub>19</sub>H<sub>16</sub>BrFN<sub>5</sub>S (M + H)<sup>+</sup>, 444.0294; found, 444.0281.

**2-((3-Bromobenzyl)thio)-N-(4-fluorophenyl)-5-methyl-[1,2,4]triazolo[1,5-*a*]pyrimidin-7-amine (13).** White solid, yield: 84%. HPLC purity: 99.85%. m.p.: 208–213 °C. <sup>1</sup>H NMR (400 MHz, DMSO-*d*<sub>6</sub>) δ 7.77 (s, 1H), 7.57–7.43 (m, 4H), 7.38 (t, *J* = 8.8 Hz, 2H), 7.29 (t, *J* = 7.8 Hz, 1H), 6.37 (s, 1H), 4.56 (s, 2H), 2.45 (s, 3H). <sup>13</sup>C NMR (100 MHz, DMSO-*d*<sub>6</sub>) δ 164.84, 161.89, 160.39, 159.46, 152.57, 146.59, 140.80, 131.99, 131.66, 130.57, 130.16, 128.08, 127.55, 127.46, 121.50, 116.66, 116.44, 90.36, 33.69, 22.10. HRMS (ESI): *m/z* calcd for C<sub>19</sub>H<sub>16</sub>BrFN<sub>5</sub>S (M + H)<sup>+</sup>, 444.0294; found, 444.0281.

**N-(4-Fluorophenyl)-5-methyl-2-((4-(trifluoromethyl)benzyl)thio)-[1,2,4]triazolo[1,5-*a*]pyrimidin-7-amine (14).** White solid, yield: 89%. HPLC purity: 98.26%. m.p.: 180–188 °C. <sup>1</sup>H NMR (400 MHz, DMSO-*d*<sub>6</sub>) δ 7.73 (dd, *J* = 28.3, 8.1 Hz, 4H), 7.49 (dd, *J* = 8.8, 4.9 Hz, 2H), 7.37 (t, *J* = 8.7 Hz, 2H), 6.36 (s, 1H), 4.65 (s, 2H), 2.45 (s, 3H). <sup>13</sup>C NMR (100 MHz, DMSO-*d*<sub>6</sub>) δ 164.71, 161.86, 160.63, 159.43, 152.79, 146.53, 143.02, 132.06, 129.76, 127.98, 127.67, 127.52, 127.44, 125.54, 125.28, 125.24, 122.84, 116.63, 116.40, 90.31, 33.81, 22.23. HRMS (ESI): *m/z* calcd for C<sub>20</sub>H<sub>16</sub>F<sub>4</sub>N<sub>5</sub>S (M + H)<sup>+</sup>, 434.1063; found, 434.1062.

**N-(4-Fluorophenyl)-5-methyl-2-((4-nitrobenzyl)thio)-[1,2,4]triazolo[1,5-*a*]pyrimidin-7-amine (15).** White solid, yield: 92%. HPLC purity: 99.28%. m.p.: 171–175 °C. <sup>1</sup>H NMR (400 MHz, CDCl<sub>3</sub>) δ 8.13 (d, *J* = 8.7 Hz, 2H), 7.73–7.53 (m, 3H), 7.32 (dd, *J* = 8.8, 4.6 Hz, 2H), 7.18 (t, *J* = 8.4 Hz, 2H), 6.16 (s, 1H), 4.59 (s, 2H), 2.51 (s, 3H). <sup>13</sup>C NMR (100 MHz, CDCl<sub>3</sub>) δ 165.48, 165.10, 162.60, 160.13, 155.79, 147.16, 145.82, 144.86, 131.34, 129.92, 126.59, 126.51, 123.70, 117.19, 116.96, 89.01, 34.77, 25.38. HRMS (ESI): *m/z* calcd for C<sub>19</sub>H<sub>16</sub>FN<sub>5</sub>O<sub>2</sub>S (M + H)<sup>+</sup>, 411.1039; found, 411.1024.

**N-(4-Fluorophenyl)-5-methyl-2-((3-nitrobenzyl)thio)-[1,2,4]triazolo[1,5-*a*]pyrimidin-7-amine (16).** White solid, yield: 88%. HPLC purity: 99.28%. m.p.: 162–167 °C. <sup>1</sup>H NMR (400 MHz, DMSO-*d*<sub>6</sub>) δ 7.69 (s, 1H), 7.54–7.41 (m, 2H), 7.30 (d, *J* = 7.8 Hz, 1H), 6.84 (t, *J* = 8.7 Hz, 2H), 6.55 (dd, *J* = 7.9, 4.9 Hz, 2H), 5.82 (s, 1H), 4.44 (s, 2H), 2.30 (s, 3H). <sup>13</sup>C NMR (100 MHz, DMSO-*d*<sub>6</sub>) δ 162.16, 155.85, 155.31, 153.56, 151.73, 151.29, 145.54, 141.09, 132.00, 131.04, 130.61, 128.42, 122.00, 115.65, 115.43, 115.14, 115.07, 99.04, 34.22, 19.03. HRMS (ESI): *m/z* calcd for C<sub>19</sub>H<sub>16</sub>FN<sub>5</sub>O<sub>2</sub>S (M + H)<sup>+</sup>, 411.1039; found, 411.1024.

**2-((2,6-Dichlorobenzyl)thio)-N-(4-fluorophenyl)-5-methyl-[1,2,4]triazolo[1,5-*a*]pyrimidin-7-amine (17).** White solid, yield: 77%. HPLC purity: 98.85%. m.p.: 200–206 °C. <sup>1</sup>H NMR (400 MHz, DMSO-*d*<sub>6</sub>) δ 7.56 (d, *J* = 8.1 Hz, 2H), 7.52–7.32 (m, 5H), 6.38 (s, 1H), 4.86 (s, 2H), 2.46 (s, 3H). <sup>13</sup>C NMR (100 MHz, DMSO-*d*<sub>6</sub>) δ 164.42, 161.75, 160.05, 159.33, 146.41, 135.12, 132.21, 131.83, 130.66, 128.86, 127.36, 127.27, 116.60, 116.38, 90.22, 31.58, 22.64. HRMS (ESI): *m/z* calcd for C<sub>19</sub>H<sub>15</sub>Cl<sub>2</sub>FN<sub>5</sub>S (M + H)<sup>+</sup>, 434.0409; found, 434.0396.

**N-(4-Fluorophenyl)-5-methyl-2-((4-methylbenzyl)thio)-[1,2,4]triazolo[1,5-*a*]pyrimidin-7-amine (18).** White solid, yield: 86%. HPLC purity: 98.99%. m.p.: 171–174 °C. <sup>1</sup>H NMR (400 MHz, DMSO-*d*<sub>6</sub>) δ 7.49 (dd, *J* = 8.9, 4.9 Hz, 2H), 7.38 (dd, *J* = 12.1, 5.3 Hz, 4H), 7.13 (d, *J* = 7.9 Hz, 2H), 6.38 (s, 1H), 4.53 (s, 2H), 2.46 (s, 3H), 2.27 (s, 3H). <sup>13</sup>C NMR (100 MHz, DMSO-*d*<sub>6</sub>) δ 165.28, 161.92, 160.05, 159.49, 152.26, 146.68, 136.60, 134.37, 131.96, 131.93, 129.03, 128.87, 127.56, 127.47, 116.66, 116.43, 90.41, 34.43, 21.87, 20.66. HRMS (ESI): *m/z* calcd for C<sub>20</sub>H<sub>19</sub>FN<sub>5</sub>S (M + H)<sup>+</sup>, 380.1345; found, 380.1332.

**N-(4-Fluorophenyl)-2-((4-methoxybenzyl)thio)-5-methyl-[1,2,4]triazolo[1,5-*a*]pyrimidin-7-amine (19).** White solid, yield: 91%. HPLC purity: 96.78%. m.p.: 168–172 °C. <sup>1</sup>H NMR (400 MHz, DMSO-*d*<sub>6</sub>) δ 7.37 (d, *J* = 8.2 Hz, 2H), 6.93–6.79 (m, 4H), 6.55 (dd, *J* = 7.8, 5.1 Hz, 2H), 5.82 (s, 1H), 4.39 (s, 2H), 3.73 (s, 3H), 2.30 (s, 3H). <sup>13</sup>C NMR (100 MHz, DMSO-*d*<sub>6</sub>) δ 162.61, 159.02, 155.85, 155.34, 153.56, 151.66, 151.22, 145.55, 130.57, 129.59, 115.65, 115.43, 115.14, 115.07, 114.35, 98.99, 55.53, 34.63, 19.02. HRMS (ESI): *m/z* calcd for C<sub>20</sub>H<sub>19</sub>FN<sub>5</sub>OS (M + H)<sup>+</sup>, 396.1294; found, 396.1280.

*N*-(4-Fluorophenyl)-5-methyl-2-((naphthalen-1-ylmethyl)thio)-[1,2,4]triazolo[1,5-*a*]pyrimidin-7-amine (**20**). White solid, yield: 81%. HPLC purity: 99.22%. m.p.: 183–187 °C. <sup>1</sup>H NMR (400 MHz, DMSO-*d*<sub>6</sub>) δ 8.21 (d, *J* = 8.2 Hz, 1H), 7.98 (d, *J* = 7.8 Hz, 1H), 7.89 (d, *J* = 8.2 Hz, 1H), 7.77 (d, *J* = 6.9 Hz, 1H), 7.66–7.34 (m, 7H), 6.38 (s, 1H), 5.09 (s, 2H), 2.47 (s, 3H). <sup>13</sup>C NMR (100 MHz, DMSO-*d*<sub>6</sub>) δ 165.18, 161.87, 160.54, 159.44, 152.70, 146.57, 133.49, 132.61, 132.03, 130.89, 128.73, 128.39, 127.77, 127.51, 127.42, 126.49, 126.01, 125.48, 123.71, 116.65, 116.42, 90.33, 32.65, 22.20. HRMS (ESI): *m/z* calcd for C<sub>23</sub>H<sub>19</sub>FN<sub>5</sub>S (M + H)<sup>+</sup>, 416.1345; found, 416.1330.

*N*-(4-Fluorophenyl)-5-methyl-2-(phenethylthio)-[1,2,4]triazolo[1,5-*a*]pyrimidin-7-amine (**21**). White solid, yield: 79%. HPLC purity: 97.05%. m.p.: 201–203 °C. <sup>1</sup>H NMR (400 MHz, DMSO-*d*<sub>6</sub>) δ 7.38–7.20 (m, 5H), 6.84 (t, *J* = 8.9 Hz, 2H), 6.55 (m, 2H), 5.82 (s, 1H), 3.41 (t, *J* = 7.5 Hz, 2H), 3.04 (t, *J* = 7.5 Hz, 2H), 2.31 (s, 3H). <sup>13</sup>C NMR (100 MHz, DMSO-*d*<sub>6</sub>) δ 162.65, 155.85, 155.36, 153.57, 151.70, 151.15, 145.56, 140.39, 129.03, 128.83, 126.83, 115.64, 115.43, 115.14, 115.07, 98.97, 35.59, 32.40, 19.01. HRMS (ESI): *m/z* calcd for C<sub>20</sub>H<sub>19</sub>FN<sub>5</sub>S (M + H)<sup>+</sup>, 380.1345; found, 380.1332.

*N*-(4-Fluorophenyl)-5-methyl-2-((3-phenylpropyl)thio)-[1,2,4]triazolo[1,5-*a*]pyrimidin-7-amine (**22**). White solid, yield: 81%. HPLC purity: 99.82%. m.p.: 172–175 °C. <sup>1</sup>H NMR (400 MHz, DMSO-*d*<sub>6</sub>) δ 7.52–7.45 (m, 2H), 7.37 (m, 2H), 7.23 (m, 5H), 6.37 (s, 1H), 3.29 (t, *J* = 7.1 Hz, 2H), 2.80–2.70 (m, 2H), 2.46 (s, 3H), 2.14–2.00 (m, 2H). <sup>13</sup>C NMR (100 MHz, DMSO-*d*<sub>6</sub>) δ 165.53, 161.95, 159.75, 159.53, 152.09, 146.76, 141.03, 131.92, 128.34, 128.29, 127.62, 127.54, 125.89, 116.67, 116.44, 90.43, 33.91, 30.91, 30.42, 21.71. HRMS (ESI): *m/z* calcd for C<sub>21</sub>H<sub>21</sub>FN<sub>5</sub>S (M + H)<sup>+</sup>, 394.1502; found, 394.1489.

*N*-(4-Fluorophenyl)-5-methyl-2-(propylthio)-[1,2,4]triazolo[1,5-*a*]pyrimidin-7-amine (**23**). White solid, yield: 83%. HPLC purity: 99.57%. m.p.: 187–192 °C. <sup>1</sup>H NMR (400 MHz, CDCl<sub>3</sub>) δ 7.66 (s, 1H), 7.39–7.30 (m, 2H), 7.23–7.14 (m, 2H), 6.14 (s, 1H), 3.31–3.20 (m, 2H), 2.49 (s, 3H), 1.91–1.77 (m, 2H), 1.05 (t, *J* = 7.4 Hz, 3H). <sup>13</sup>C NMR (100 MHz, CDCl<sub>3</sub>) δ 167.26, 164.67, 162.46, 160.01, 155.92, 144.67, 131.60, 126.54, 126.46, 117.09, 116.86, 88.62, 33.44, 25.33, 23.28, 13.34. HRMS (ESI): *m/z* calcd for C<sub>15</sub>H<sub>17</sub>FN<sub>5</sub>S (M + H)<sup>+</sup>, 318.1189; found, 318.1178.

2-(((1*H*-Benzo[d]imidazol-2-yl)methyl)thio)-*N*-(4-fluorophenyl)-5-methyl-1,2,4-triazolo[1,5-*a*]pyrimidin-7-amine (**24**). White solid, yield: 81%. HPLC purity: 99.17%. m.p.: 203–208 °C. <sup>1</sup>H NMR (400 MHz, DMSO-*d*<sub>6</sub>) δ 7.43 (m, 2H), 7.28 (m, 2H), 6.20 (s, 1H), 5.99 (m, 1H), 5.31 (dd, *J* = 17.0, 1.2 Hz, 1H), 5.08 (d, *J* = 10.0 Hz, 1H), 3.90 (d, *J* = 6.9 Hz, 2H), 2.33 (s, 3H). <sup>13</sup>C NMR (100 MHz, DMSO-*d*<sub>6</sub>) δ 164.32, 163.95, 155.78, 145.25, 133.96, 132.97, 127.02, 126.93, 118.06, 116.38, 116.15, 89.12, 33.27, 24.64. HRMS (ESI): *m/z* calcd for C<sub>15</sub>H<sub>15</sub>FN<sub>5</sub>S (M + H)<sup>+</sup>, 316.1032; found, 316.1031.

*N*-(4-Fluorophenyl)-5-methyl-2-(prop-2-yn-1-ylthio)-[1,2,4]triazolo[1,5-*a*]pyrimidin-7-amine (**25**). White solid, yield: 74%. HPLC purity: 99.86%. m.p.: 201–205 °C. <sup>1</sup>H NMR (400 MHz, DMSO-*d*<sub>6</sub>) δ 7.57–7.45 (m, 2H), 7.37 (m, 2H), 6.38 (s, 1H), 4.17 (d, *J* = 2.5 Hz, 2H), 3.28 (t, *J* = 2.5 Hz, 1H), 2.45 (s, 3H). <sup>13</sup>C NMR (100 MHz, DMSO-*d*<sub>6</sub>) δ 164.05, 162.20, 161.15, 159.39, 152.95, 146.56, 127.42, 127.33, 116.64, 116.41, 90.33, 79.95, 74.17, 22.37, 19.26. HRMS (ESI): *m/z* calcd for C<sub>15</sub>H<sub>13</sub>FN<sub>5</sub>S (M + H)<sup>+</sup>, 314.0876; found, 314.0877.

2-(((Cyclopropylmethyl)thio)-*N*-(4-fluorophenyl)-5-methyl-1,2,4-triazolo[1,5-*a*]pyrimidin-7-amine (**26**). White solid, yield: 80%. HPLC purity: 98.10%. m.p.: 175–182 °C. <sup>1</sup>H NMR (400 MHz, CDCl<sub>3</sub>) δ 7.68 (s, 1H), 7.35 (dd, *J* = 8.8, 4.7 Hz, 2H), 7.19 (t, *J* = 8.5 Hz, 2H), 6.14 (s, 1H), 3.24 (d, *J* = 7.3 Hz, 2H), 2.49 (s, 3H), 1.29–1.18 (m, 1H), 0.65–0.55 (m, 2H), 0.40–0.30 (m, 2H). <sup>13</sup>C NMR (100 MHz, CDCl<sub>3</sub>) δ 167.27, 164.70, 162.47, 160.01, 155.89, 144.68, 131.63, 131.60, 126.55, 126.47, 117.09, 116.86, 88.65, 37.39, 25.34, 11.19, 5.92. HRMS (ESI): *m/z* calcd for C<sub>16</sub>H<sub>17</sub>FN<sub>5</sub>S (M + H)<sup>+</sup>, 330.1189; found, 330.1177.

2-(((1*H*-Benzo[d]imidazol-2-yl)methyl)thio)-*N*-(4-fluorophenyl)-5-methyl-1,2,4-triazolo[1,5-*a*]pyrimidin-7-amine (**27**). White solid, yield: 91%. HPLC purity: 99.33%. m.p.: 207–215 °C. <sup>1</sup>H NMR (400 MHz, DMSO-*d*<sub>6</sub>) δ 7.63 (m, 2H), 7.49 (m, 2H), 7.43–7.30 (m, 4H),

6.27 (s, 1H), 4.88 (s, 2H), 2.37 (s, 3H). <sup>13</sup>C NMR (100 MHz, DMSO-*d*<sub>6</sub>) δ 164.13, 163.35, 161.32, 158.90, 155.72, 150.82, 145.29, 135.49, 132.71, 127.09, 127.00, 123.35, 116.41, 116.19, 114.48, 89.29, 27.21, 24.54. HRMS (ESI): *m/z* calcd for C<sub>20</sub>H<sub>15</sub>FN<sub>7</sub>S (M – H)<sup>+</sup>, 404.1094; found, 404.1102.

2-(((5-Chlorobenzo[*b*]thiophen-3-yl)methyl)thio)-*N*-(4-fluorophenyl)-5-methyl-1,2,4-triazolo[1,5-*a*]pyrimidin-7-amine (**28**). White solid, yield: 76%. HPLC purity: 99.48%. m.p.: 191–196 °C. <sup>1</sup>H NMR (400 MHz, DMSO-*d*<sub>6</sub>) δ 8.10 (d, *J* = 1.9 Hz, 1H), 8.03 (d, *J* = 8.6 Hz, 1H), 7.94 (s, 1H), 7.54–7.39 (m, 3H), 7.37–7.28 (m, 2H), 6.26 (s, 1H), 4.83 (s, 2H), 2.39 (s, 3H). <sup>13</sup>C NMR (100 MHz, DMSO-*d*<sub>6</sub>) δ 164.30, 164.01, 161.32, 158.90, 155.76, 145.31, 139.13, 138.23, 132.92, 131.49, 129.50, 128.43, 127.09, 127.00, 124.71, 124.54, 121.64, 116.40, 116.18, 89.20, 27.77, 24.62. HRMS (ESI): *m/z* calcd for C<sub>21</sub>H<sub>16</sub>ClFN<sub>5</sub>S<sub>2</sub> (M + H)<sup>+</sup>, 456.0520; found, 456.0503.

2-(((7-((4-Fluorophenyl)amino)-5-methyl-1,2,4-triazolo[1,5-*a*]pyrimidin-2-yl)thio)-1-phenylethan-1-one (**29**). White solid, yield: 81%. HPLC purity: 98.18%. m.p.: 201–207 °C. <sup>1</sup>H NMR (400 MHz, CDCl<sub>3</sub>) δ 8.10–8.03 (m, 2H), 7.66 (s, 1H), 7.58 (t, *J* = 7.4 Hz, 1H), 7.47 (t, *J* = 7.6 Hz, 2H), 7.36–7.30 (m, 2H), 7.21–7.13 (m, 2H), 6.12 (s, 1H), 4.89 (s, 2H), 2.46 (s, 3H). <sup>13</sup>C NMR (100 MHz, CDCl<sub>3</sub>) δ 193.60, 165.78, 164.88, 162.54, 160.07, 155.83, 144.87, 135.68, 133.66, 131.54, 131.51, 128.76, 128.56, 126.65, 126.57, 117.10, 116.87, 88.89, 39.60, 25.32. HRMS (ESI): *m/z* calcd for C<sub>20</sub>H<sub>17</sub>FN<sub>5</sub>OS (M + H)<sup>+</sup>, 394.1138; found, 394.1137.

2-(((1*H*-Benzo[*d*]imidazol-2-yl)methyl)thio)-*N*-(2-fluorophenyl)-5-methyl-1,2,4-triazolo[1,5-*a*]pyrimidin-7-amine (**30**). White solid, yield: 91%. HPLC purity: 96.76%. m.p.: 181–186 °C. <sup>1</sup>H NMR (400 MHz, DMSO-*d*<sub>6</sub>) δ 7.85–7.77 (m, 2H), 7.63–7.45 (m, 5H), 7.43–7.36 (m, 1H), 6.09 (d, *J* = 1.8 Hz, 1H), 5.09 (s, 2H), 2.40 (s, 3H). <sup>13</sup>C NMR (100 MHz, DMSO-*d*<sub>6</sub>) δ 163.26, 162.28, 158.18, 155.70, 154.04, 150.46, 146.06, 130.67, 129.89, 129.81, 129.24, 125.93, 125.44, 123.08, 122.96, 117.02, 116.83, 113.95, 90.25, 25.21, 22.95. HRMS (ESI): *m/z* calcd for C<sub>20</sub>H<sub>17</sub>FN<sub>7</sub>S (M + H)<sup>+</sup>, 406.1250; found, 406.1249.

2-(((1*H*-Benzo[*d*]imidazol-2-yl)methyl)thio)-*N*-(3-fluorophenyl)-5-methyl-1,2,4-triazolo[1,5-*a*]pyrimidin-7-amine (**31**). White solid, yield: 93%. HPLC purity: 99.92%. m.p.: 198–202 °C. <sup>1</sup>H NMR (400 MHz, DMSO-*d*<sub>6</sub>) δ 7.81 (m, 2H), 7.55 (m, 4H), 7.39 (m, 2H), 6.34 (s, 1H), 5.08 (s, 2H), 2.39 (s, 3H). <sup>13</sup>C NMR (100 MHz, DMSO-*d*<sub>6</sub>) δ 162.98, 162.13, 161.75, 159.32, 154.19, 150.57, 146.08, 132.10, 130.68, 127.60, 127.52, 125.94, 116.52, 116.29, 113.97, 89.99, 25.19, 23.06. HRMS (ESI): *m/z* calcd for C<sub>20</sub>H<sub>17</sub>FN<sub>7</sub>S (M + H)<sup>+</sup>, 406.1250; found, 406.1250.

2-(((1*H*-Benzo[*d*]imidazol-2-yl)methyl)thio)-*N*-(2,6-difluorophenyl)-5-methyl-1,2,4-triazolo[1,5-*a*]pyrimidin-7-amine (**32**). White solid, yield: 86%. HPLC purity: 98.74%. m.p.: 195–201 °C. <sup>1</sup>H NMR (400 MHz, DMSO-*d*<sub>6</sub>) δ 7.84–7.77 (m, 2H), 7.66–7.52 (m, 3H), 7.39 (t, *J* = 8.2 Hz, 2H), 6.06 (s, 1H), 5.08 (s, 2H), 2.38 (s, 3H). <sup>13</sup>C NMR (100 MHz, DMSO-*d*<sub>6</sub>) δ 163.57, 163.27, 159.70, 157.20, 154.80, 150.53, 145.59, 130.68, 130.31, 125.91, 113.91, 112.89, 112.67, 89.95, 25.29, 23.58. HRMS (ESI): *m/z* calcd for C<sub>20</sub>H<sub>16</sub>F<sub>2</sub>N<sub>7</sub>S (M + H)<sup>+</sup>, 424.1156; found, 424.1157.

2-(((1*H*-Benzo[*d*]imidazol-2-yl)methyl)thio)-*N*-(3-chloro-4-fluorophenyl)-5-methyl-1,2,4-triazolo[1,5-*a*]pyrimidin-7-amine (**33**). White solid, yield: 90.75%. HPLC purity: 99.75%. m.p.: 183–189 °C. <sup>1</sup>H NMR (400 MHz, DMSO-*d*<sub>6</sub>) δ 7.85–7.75 (m, 3H), 7.63–7.50 (m, 4H), 6.46 (s, 1H), 5.09 (s, 2H), 2.41 (s, 3H). <sup>13</sup>C NMR (100 MHz, DMSO-*d*<sub>6</sub>) δ 163.08, 162.43, 156.98, 154.53, 154.22, 150.49, 145.85, 133.15, 130.64, 127.49, 126.22, 126.14, 125.93, 120.22, 120.03, 117.79, 117.57, 113.97, 90.40, 25.12, 23.10. HRMS (ESI): *m/z* calcd for C<sub>20</sub>H<sub>16</sub>ClFN<sub>7</sub>S (M + H)<sup>+</sup>, 440.0860; found, 440.0860.

2-(((1*H*-Benzo[*d*]imidazol-2-yl)methyl)thio)-5-methyl-*N*-(2,4,5-trifluorophenyl)-1,2,4-triazolo[1,5-*a*]pyrimidin-7-amine (**34**). White solid, yield: 89%. HPLC purity: 99.22%. m.p.: 210–216 °C. <sup>1</sup>H NMR (400 MHz, DMSO-*d*<sub>6</sub>) δ 7.94–7.75 (m, 4H), 7.60–7.49 (m, 2H), 6.21 (d, *J* = 1.5 Hz, 1H), 5.07 (s, 2H), 2.38 (s, 3H). <sup>13</sup>C NMR (100 MHz, DMSO-*d*<sub>6</sub>) δ 163.49, 163.12, 156.05, 154.87, 150.56, 145.62, 140.20, 130.68, 130.54, 125.92, 117.85, 117.65,

116.86, 113.96, 107.41, 107.19, 90.36, 25.23, 23.66. HRMS (ESI):  $m/z$  calcd for  $C_{20}H_{15}F_3N_5S$  ( $M + H$ )<sup>+</sup>, 442.1062; found, 442.1062.

2-(((1*H*-Benzo[d]imidazol-2-yl)methyl)thio)-*N*-(4-fluoro-3-methylphenyl)-5-methyl-[1,2,4]triazolo[1,5-*a*]pyrimidin-7-amine (35). White solid, yield: 88%. HPLC purity: 99.17%. m.p.: 193–198 °C. <sup>1</sup>H NMR (400 MHz, DMSO-*d*<sub>6</sub>) δ 7.86–7.77 (m, 2H), 7.58–7.51 (m, 2H), 7.45–7.39 (m, 1H), 7.39–7.28 (m, 2H), 6.33 (s, 1H), 5.09 (s, 2H), 2.40 (s, 3H), 2.31 (d, *J* = 1.5 Hz, 3H). <sup>13</sup>C NMR (100 MHz, DMSO-*d*<sub>6</sub>) δ 163.08, 161.61, 160.45, 158.03, 153.80, 150.50, 146.30, 131.52, 130.67, 128.67, 128.62, 125.94, 125.78, 125.60, 125.05, 124.97, 116.09, 115.86, 113.97, 90.12, 25.16, 22.74, 14.25, 14.22. HRMS (ESI):  $m/z$  calcd for  $C_{21}H_{19}FN_7S$  ( $M + H$ )<sup>+</sup>, 420.1407; found, 420.1407.

2-(((1*H*-Benzo[d]imidazol-2-yl)methyl)thio)-*N*-(2-fluoro-4-methylphenyl)-5-methyl-[1,2,4]triazolo[1,5-*a*]pyrimidin-7-amine (36). White solid, yield: 83%. HPLC purity: 98.82%. m.p.: 202–207 °C. <sup>1</sup>H NMR (400 MHz, DMSO-*d*<sub>6</sub>) δ 7.84–7.77 (m, 2H), 7.58–7.51 (m, 2H), 7.44 (t, *J* = 8.2 Hz, 1H), 7.31 (d, *J* = 11.3 Hz, 1H), 7.20 (d, *J* = 7.6 Hz, 1H), 6.06 (d, *J* = 1.7 Hz, 1H), 5.08 (s, 2H), 2.41 (s, 3H), 2.39 (s, 3H). <sup>13</sup>C NMR (100 MHz, DMSO-*d*<sub>6</sub>) δ 163.22, 162.25, 157.94, 155.47, 154.08, 150.44, 146.20, 140.29, 140.22, 130.65, 128.90, 125.93, 120.24, 120.11, 117.26, 117.07, 113.94, 90.14, 30.65, 25.21, 22.97, 20.62. HRMS (ESI):  $m/z$  calcd for  $C_{21}H_{19}FN_7S$  ( $M + H$ )<sup>+</sup>, 420.1407; found, 420.1408.

2-(((1*H*-Benzo[d]imidazol-2-yl)methyl)thio)-5-methyl-*N*-(4-(trifluoromethyl)phenyl)-[1,2,4]triazolo[1,5-*a*]pyrimidin-7-amine (37). White solid, yield: 89%. HPLC purity: 97.45%. m.p.: 185–189 °C. <sup>1</sup>H NMR (400 MHz, DMSO-*d*<sub>6</sub>) δ 7.93 (s, 1H), 7.86 (d, *J* = 7.8 Hz, 1H), 7.83–7.70 (m, 4H), 7.58–7.49 (m, 2H), 6.52 (s, 1H), 5.10 (s, 2H), 2.42 (s, 3H). <sup>13</sup>C NMR (100 MHz, DMSO-*d*<sub>6</sub>) δ 163.04, 162.81, 154.50, 150.57, 145.42, 137.07, 130.79, 130.65, 130.36, 130.05, 128.60, 125.93, 125.12, 123.08, 122.41, 121.55, 113.95, 90.39, 25.14, 23.35. HRMS (ESI):  $m/z$  calcd for  $C_{21}H_{17}F_3N_7S$  ( $M + H$ )<sup>+</sup>, 456.1218; found, 456.1219.

2-(((1*H*-Benzo[d]imidazol-2-yl)methyl)thio)-5-methyl-*N*-(4-(trifluoromethoxy)phenyl)-[1,2,4]triazolo[1,5-*a*]pyrimidin-7-amine (38). White solid, yield: 82%. HPLC purity: 99.07%. m.p.: 203–207 °C. <sup>1</sup>H NMR (400 MHz, DMSO-*d*<sub>6</sub>) δ 7.81 (m, 2H), 7.66 (d, *J* = 8.9 Hz, 2H), 7.54 (m, 4H), 6.48 (s, 1H), 5.09 (s, 2H), 2.41 (s, 3H). <sup>13</sup>C NMR (100 MHz, DMSO-*d*<sub>6</sub>) δ 162.94, 162.84, 154.59, 150.64, 146.20, 145.43, 135.23, 130.67, 126.69, 125.93, 124.50, 122.21, 121.34, 118.79, 113.96, 101.15, 90.12, 25.16, 23.41. HRMS (ESI):  $m/z$  calcd for  $C_{21}H_{17}F_3N_7S$  ( $M + H$ )<sup>+</sup>, 456.1218; found, 456.1213.

2-(((1*H*-Benzo[d]imidazol-2-yl)methyl)thio)-5-methyl-*N*-phenyl-[1,2,4]triazolo[1,5-*a*]pyrimidin-7-amine (39). White solid, yield: 79%. HPLC purity: 99.37%. m.p.: 180–191 °C. <sup>1</sup>H NMR (400 MHz, DMSO-*d*<sub>6</sub>) δ 7.50 (m, 6H), 7.33 (d, *J* = 7.0 Hz, 1H), 7.18 (m, 2H), 6.34 (s, 1H), 4.79 (s, 2H), 2.38 (s, 3H). <sup>13</sup>C NMR (100 MHz, DMSO-*d*<sub>6</sub>) δ 164.03, 163.80, 155.80, 150.66, 144.94, 136.53, 129.48, 126.12, 124.44, 122.01, 114.75, 89.29, 28.00, 24.60. HRMS (ESI):  $m/z$  calcd for  $C_{20}H_{16}N_7S$  ( $M - H$ )<sup>+</sup>, 386.1188; found, 386.1196.

2-(((1*H*-Benzo[d]imidazol-2-yl)methyl)thio)-*N*-(4-chlorophenyl)-5-methyl-[1,2,4]triazolo[1,5-*a*]pyrimidin-7-amine (40). White solid, yield: 81%. HPLC purity: 97.17%. m.p.: 213–217 °C. <sup>1</sup>H NMR (400 MHz, DMSO-*d*<sub>6</sub>) δ 7.78 (m, 2H), 7.61–7.48 (m, 6H), 6.45 (s, 1H), 5.07 (s, 2H), 2.39 (s, 3H). <sup>13</sup>C NMR (100 MHz, DMSO-*d*<sub>6</sub>) δ 163.11, 161.84, 153.87, 150.47, 145.79, 134.79, 131.02, 130.63, 129.53, 126.89, 125.94, 113.95, 90.39, 25.12, 22.77. HRMS (ESI):  $m/z$  calcd for  $C_{20}H_{15}ClN_7S$  ( $M - H$ )<sup>+</sup>, 420.0798; found, 420.0807.

2-(((1*H*-Benzo[d]imidazol-2-yl)methyl)thio)-*N*-(4-bromophenyl)-5-methyl-[1,2,4]triazolo[1,5-*a*]pyrimidin-7-amine (41). White solid, yield: 78%. HPLC purity: 100%. m.p.: 206–210 °C. <sup>1</sup>H NMR (400 MHz, DMSO-*d*<sub>6</sub>) δ 7.66 (d, *J* = 8.7 Hz, 2H), 7.56–7.47 (m, 2H), 7.42 (d, *J* = 8.7 Hz, 2H), 7.15 (s, 1H), 6.42 (s, 1H), 4.77 (s, 2H), 2.40 (s, 3H). <sup>13</sup>C NMR (100 MHz, DMSO-*d*<sub>6</sub>) δ 164.24, 164.06, 155.84, 150.61, 144.67, 136.19, 132.38, 126.38, 121.74, 118.26, 89.70, 28.34, 24.66. HRMS (ESI):  $m/z$  calcd for  $C_{20}H_{17}BrN_7S$  ( $M + H$ )<sup>+</sup>, 466.0450; found, 466.0277.

4-((2-(((1*H*-Benzo[d]imidazol-2-yl)methyl)thio)-5-methyl-[1,2,4]triazolo[1,5-*a*]pyrimidin-7-yl)amino)benzoic acid (42). White solid, yield: 85%. HPLC purity: 98.45%. m.p.: 230–235 °C. <sup>1</sup>H NMR (400

MHz, DMSO-*d*<sub>6</sub>) δ 8.07 (d, *J* = 8.5 Hz, 2H), 7.81 (m, 2H), 7.69 (d, *J* = 8.5 Hz, 2H), 7.54 (dd, *J* = 6.2, 3.1 Hz, 2H), 6.64 (s, 1H), 5.11 (s, 2H), 2.44 (s, 3H). <sup>13</sup>C NMR (100 MHz, DMSO-*d*<sub>6</sub>) δ 166.64, 163.04, 162.70, 154.38, 150.60, 145.01, 140.26, 130.67, 130.64, 128.25, 125.94, 123.94, 113.96, 90.88, 25.15, 23.25. HRMS (ESI):  $m/z$  calcd for  $C_{21}H_{16}N_7O_2S$  ( $M - H$ )<sup>+</sup>, 430.1086; found, 430.1094.

4-((2-(((1*H*-Benzo[d]imidazol-2-yl)methyl)thio)-5-methyl-[1,2,4]triazolo[1,5-*a*]pyrimidin-7-yl)amino)benzotrile (43). White solid, yield: 89%. HPLC purity: 98.96%. m.p.: 236–239 °C. <sup>1</sup>H NMR (400 MHz, DMSO-*d*<sub>6</sub>) δ 7.96 (d, *J* = 8.6 Hz, 2H), 7.85–7.73 (m, 4H), 7.51 (m, 2H), 6.68 (s, 1H), 5.08 (s, 2H), 2.42 (s, 3H). <sup>13</sup>C NMR (100 MHz, DMSO-*d*<sub>6</sub>) δ 163.02, 154.48, 150.51, 144.49, 140.88, 133.59, 130.55, 125.86, 124.23, 118.54, 113.88, 107.87, 91.25, 25.04, 23.34. HRMS (ESI):  $m/z$  calcd for  $C_{21}H_{15}N_8S$  ( $M - H$ )<sup>+</sup>, 411.1140; found, 411.1148.

1-(4-((2-(((1*H*-Benzo[d]imidazol-2-yl)methyl)thio)-5-methyl-[1,2,4]triazolo[1,5-*a*]pyrimidin-7-yl)amino)phenyl)ethan-1-one (44). White solid, yield: 82%. HPLC purity: 99.44%. m.p.: 183–186 °C. <sup>1</sup>H NMR (400 MHz, DMSO-*d*<sub>6</sub>) δ 8.05 (d, *J* = 8.4 Hz, 2H), 7.63 (d, *J* = 8.4 Hz, 2H), 7.56 (m, 2H), 7.22 (m, 2H), 6.65 (s, 1H), 4.84 (s, 2H), 2.60 (s, 3H), 2.44 (s, 3H). <sup>13</sup>C NMR (100 MHz, DMSO-*d*<sub>6</sub>) δ 196.70, 163.90, 161.23, 155.90, 150.70, 143.95, 141.51, 133.52, 129.70, 122.80, 122.45, 114.74, 90.67, 27.75, 26.62, 24.69. HRMS (ESI):  $m/z$  calcd for  $C_{22}H_{20}N_7OS$  ( $M + H$ )<sup>+</sup>, 430.1450; found, 430.1451.

2-(((1*H*-Benzo[d]imidazol-2-yl)methyl)thio)-*N*-(2,4-dichlorophenyl)-5-methyl-[1,2,4]triazolo[1,5-*a*]pyrimidin-7-amine (45). White solid, yield: 76%. HPLC purity: 96.90%. m.p.: 170–176 °C. <sup>1</sup>H NMR (400 MHz, DMSO-*d*<sub>6</sub>) δ 7.91 (d, *J* = 1.5 Hz, 1H), 7.84–7.76 (m, 2H), 7.66–7.60 (m, 2H), 7.58–7.51 (m, 2H), 6.00 (s, 1H), 5.08 (s, 2H), 2.36 (s, 3H). <sup>13</sup>C NMR (100 MHz, DMSO-*d*<sub>6</sub>) δ 163.11, 162.90, 154.57, 150.54, 145.72, 133.32, 132.54, 132.21, 131.24, 130.67, 130.05, 128.81, 125.92, 113.95, 90.37, 25.30, 23.35. HRMS (ESI):  $m/z$  calcd for  $C_{20}H_{16}Cl_2N_7S$  ( $M + H$ )<sup>+</sup>, 456.0565; found, 456.0564.

2-(((1*H*-Benzo[d]imidazol-2-yl)methyl)thio)-5-methyl-*N*-(*p*-tolyl)-[1,2,4]triazolo[1,5-*a*]pyrimidin-7-amine (46). White solid, yield: 86%. HPLC purity: 99.06%. m.p.: 240–247 °C. <sup>1</sup>H NMR (400 MHz, DMSO-*d*<sub>6</sub>) δ 7.79 (s, 2H), 7.53 (s, 2H), 7.37 (t, *J* = 6.7 Hz, 4H), 6.37 (s, 1H), 5.09 (s, 2H), 2.41 (s, 3H), 2.37 (s, 3H). <sup>13</sup>C NMR (100 MHz, DMSO-*d*<sub>6</sub>) δ 163.37, 152.43, 150.23, 146.66, 136.98, 132.59, 130.62, 130.10, 125.96, 125.35, 125.17, 113.96, 90.51, 25.10, 21.51, 20.64. HRMS (ESI):  $m/z$  calcd for  $C_{21}H_{18}N_7S$  ( $M - H$ )<sup>+</sup>, 400.1344; found, 400.1352.

2-(((1*H*-Benzo[d]imidazol-2-yl)methyl)thio)-*N*-(4-methoxyphenyl)-5-methyl-[1,2,4]triazolo[1,5-*a*]pyrimidin-7-amine (47). White solid, yield: 82%. HPLC purity: 99.14%. m.p.: 213–219 °C. <sup>1</sup>H NMR (400 MHz, DMSO-*d*<sub>6</sub>) δ 7.84–7.78 (m, 2H), 7.59–7.51 (m, 2H), 7.50–7.43 (m, 1H), 7.40 (dd, *J* = 7.8, 1.5 Hz, 1H), 7.27 (d, *J* = 7.7 Hz, 1H), 7.11 (dd, *J* = 11.8, 4.3 Hz, 1H), 5.93 (s, 1H), 5.08 (s, 2H), 3.80 (s, 3H), 2.37 (s, 3H). <sup>13</sup>C NMR (100 MHz, DMSO-*d*<sub>6</sub>) δ 163.18, 161.22, 154.32, 153.69, 150.54, 146.35, 130.72, 129.46, 128.23, 125.93, 123.35, 120.96, 113.98, 112.95, 90.48, 55.72, 25.30, 22.65. HRMS (ESI):  $m/z$  calcd for  $C_{21}H_{20}N_7OS$  ( $M + H$ )<sup>+</sup>, 418.1450; found, 418.1451.

2-(((1*H*-Benzo[d]imidazol-2-yl)methyl)thio)-*N*-(3-methoxyphenyl)-5-methyl-[1,2,4]triazolo[1,5-*a*]pyrimidin-7-amine (48). White solid, yield: 80%. HPLC purity: 98.55%. m.p.: 203–208 °C. <sup>1</sup>H NMR (400 MHz, DMSO-*d*<sub>6</sub>) δ 7.81 (m, 2H), 7.54 (m, 2H), 7.45 (t, *J* = 8.1 Hz, 1H), 7.11 (m, 2H), 6.98 (m, 1H), 6.48 (s, 1H), 5.10 (s, 2H), 3.82 (s, 3H), 2.43 (s, 3H). <sup>13</sup>C NMR (100 MHz, DMSO-*d*<sub>6</sub>) δ 163.10, 161.54, 160.00, 153.72, 150.50, 145.92, 136.81, 130.65, 130.37, 125.93, 116.95, 113.96, 112.47, 110.99, 90.47, 55.98, 55.33, 25.14, 22.67, 18.52. HRMS (ESI):  $m/z$  calcd for  $C_{21}H_{20}N_7OS$  ( $M + H$ )<sup>+</sup>, 418.1450; found, 418.1451.

2-(((1*H*-Benzo[d]imidazol-2-yl)methyl)thio)-5-methyl-*N*-(3,4,5-trimethoxyphenyl)-[1,2,4]triazolo[1,5-*a*]pyrimidin-7-amine (49). White solid, yield: 88%. HPLC purity: 99.64%. m.p.: 228–235 °C. <sup>1</sup>H NMR (400 MHz, DMSO-*d*<sub>6</sub>) δ 7.80 (m, 2H), 7.53 (m, 2H), 6.84 (s, 2H), 6.52 (s, 1H), 5.08 (s, 2H), 3.81 (s, 6H), 3.72 (s, 3H), 2.41 (s,

3H).  $^{13}\text{C}$  NMR (100 MHz,  $\text{DMSO-}d_6$ )  $\delta$  163.05, 153.91, 153.24, 150.54, 145.99, 136.19, 131.32, 130.66, 125.93, 113.97, 103.01, 90.51, 60.09, 56.07, 25.16, 22.84. HRMS (ESI):  $m/z$  calcd for  $\text{C}_{23}\text{H}_{22}\text{N}_7\text{O}_3\text{S}$  ( $\text{M} + \text{H}$ ) $^+$ , 476.1505; found, 476.1513.

4-((2-(((1H-Benzo[d]imidazol-2-yl)methyl)thio)-5-methyl-[1,2,4]-triazolo[1,5-a]pyrimidin-7-yl)amino)phenol (**50**). White solid, yield: 76%. HPLC purity: 100%. m.p.: 206–212 °C.  $^1\text{H}$  NMR (400 MHz,  $\text{DMSO-}d_6$ )  $\delta$  7.82 (m, 2H), 7.54 (m, 2H), 7.28 (d,  $J = 8.7$  Hz, 2H), 6.97 (d,  $J = 8.7$  Hz, 2H), 6.27 (s, 1H), 5.10 (s, 2H), 2.42 (s, 3H).  $^{13}\text{C}$  NMR (100 MHz,  $\text{DMSO-}d_6$ )  $\delta$  163.26, 159.57, 157.01, 152.51, 150.28, 147.00, 130.65, 127.13, 125.95, 116.18, 113.97, 90.31, 25.17, 21.60. HRMS (ESI):  $m/z$  calcd for  $\text{C}_{20}\text{H}_{18}\text{N}_7\text{OS}$  ( $\text{M} + \text{H}$ ) $^+$ , 404.1294; found, 404.1293.

4-((2-(((1H-Benzo[d]imidazol-2-yl)methyl)thio)-5-methyl-[1,2,4]-triazolo[1,5-a]pyrimidin-7-yl)amino)-2-chlorophenol (**51**). White solid, yield: 83%. HPLC purity: 95.75%. m.p.: 218–225 °C.  $^1\text{H}$  NMR (400 MHz,  $\text{DMSO-}d_6$ )  $\delta$  7.82 (m, 2H), 7.54 (m, 2H), 7.46 (d,  $J = 2.5$  Hz, 1H), 7.26 (m, 1H), 7.20 (d,  $J = 8.7$  Hz, 1H), 6.30 (s, 1H), 5.08 (s, 2H), 2.40 (s, 3H).  $^{13}\text{C}$  NMR (100 MHz,  $\text{DMSO-}d_6$ )  $\delta$  163.08, 161.25, 154.07, 153.57, 152.61, 150.47, 146.59, 130.68, 127.35, 127.11, 125.95, 125.76, 119.95, 117.12, 113.98, 90.20, 25.21, 22.53. HRMS (ESI):  $m/z$  calcd for  $\text{C}_{20}\text{H}_{17}\text{ClN}_7\text{OS}$  ( $\text{M} + \text{H}$ ) $^+$ , 438.0904; found, 438.0905.

2-(((1H-Benzo[d]imidazol-2-yl)methyl)thio)-N-(3-ethynylphenyl)-5-methyl-[1,2,4]triazolo[1,5-a]pyrimidin-7-amine (**52**). White solid, yield: 78%. HPLC purity: 98.92%. m.p.: 226–231 °C.  $^1\text{H}$  NMR (400 MHz,  $\text{DMSO-}d_6$ )  $\delta$  7.86–7.79 (m, 2H), 7.63 (s, 1H), 7.61–7.46 (m, 5H), 6.45 (s, 1H), 5.10 (s, 2H), 4.37 (s, 1H), 2.42 (s, 3H).  $^{13}\text{C}$  NMR (100 MHz,  $\text{DMSO-}d_6$ )  $\delta$  163.07, 162.10, 154.06, 150.53, 145.76, 136.27, 130.65, 130.05, 128.01, 125.94, 125.73, 122.98, 113.96, 90.37, 82.66, 81.84, 25.13, 22.96. HRMS (ESI):  $m/z$  calcd for  $\text{C}_{22}\text{H}_{18}\text{N}_7\text{S}$  ( $\text{M} + \text{H}$ ) $^+$ , 412.1344; found, 412.1345.

2-(((1H-Benzo[d]imidazol-2-yl)methyl)thio)-5-methyl-N-(4-(4-methylpiperazin-1-yl)phenyl)-[1,2,4]triazolo[1,5-a]pyrimidin-7-amine (**53**). White solid, yield: 83%. HPLC purity: 97.52%. m.p.: 168–172 °C.  $^1\text{H}$  NMR (400 MHz,  $\text{DMSO-}d_6$ )  $\delta$  7.77 (m, 2H), 7.50 (m, 2H), 7.36 (d,  $J = 8.7$  Hz, 2H), 7.13 (d,  $J = 8.8$  Hz, 2H), 6.17 (s, 1H), 5.03 (s, 2H), 3.87 (s, 2H), 3.51 (s, 2H), 3.19 (s, 4H), 2.83 (s, 3H), 2.34 (s, 3H).  $^{13}\text{C}$  NMR (100 MHz,  $\text{DMSO-}d_6$ )  $\delta$  163.80, 162.68, 155.85, 150.89, 148.12, 145.69, 131.74, 128.16, 126.26, 125.37, 116.58, 114.07, 89.18, 51.98, 45.33, 41.87, 25.57, 24.43. HRMS (ESI):  $m/z$  calcd for  $\text{C}_{25}\text{H}_{28}\text{N}_9\text{S}$  ( $\text{M} + \text{H}$ ) $^+$ , 486.2188; found, 486.2148.

7-(((1H-Benzo[d]imidazol-2-yl)methyl)thio)-5-methyl-[1,2,4]-triazolo[1,5-a]pyrimidin-7-ylamino)-4-methyl-2H-chromen-2-one (**54**). White solid, yield: 87%. HPLC purity: 98.20%. m.p.: 202–211 °C.  $^1\text{H}$  NMR (400 MHz,  $\text{DMSO-}d_6$ )  $\delta$  7.88 (d,  $J = 9.2$  Hz, 1H), 7.81 (m, 2H), 7.60 (m, 2H), 7.54 (m, 2H), 6.73 (s, 1H), 6.42 (d,  $J = 1.1$  Hz, 1H), 5.11 (s, 2H), 2.47 (d,  $J = 0.8$  Hz, 3H), 2.45 (s, 3H).  $^{13}\text{C}$  NMR (100 MHz,  $\text{DMSO-}d_6$ )  $\delta$  163.23, 163.00, 159.64, 154.70, 153.51, 152.89, 150.63, 144.64, 139.68, 130.64, 126.38, 125.93, 119.81, 117.33, 113.95, 113.59, 111.16, 91.15, 25.15, 23.56, 18.06. HRMS (ESI):  $m/z$  calcd for  $\text{C}_{24}\text{H}_{20}\text{N}_7\text{O}_2\text{S}$  ( $\text{M} + \text{H}$ ) $^+$ , 470.1399; found, 470.1355.

2-(((1H-Benzo[d]imidazol-2-yl)methyl)thio)-5-methyl-N-(5-methyl-1H-pyrazol-3-yl)-[1,2,4]triazolo[1,5-a]pyrimidin-7-amine (**55**). White solid, yield: 87%. HPLC purity: 97.87%. m.p.: 206–213 °C.  $^1\text{H}$  NMR (400 MHz,  $\text{DMSO-}d_6$ )  $\delta$  7.80 (m, 2H), 7.61–7.47 (m, 2H), 7.39 (s, 1H), 6.39 (s, 1H), 5.11 (s, 2H), 2.49 (s, 3H), 2.30 (s, 3H).  $^{13}\text{C}$  NMR (100 MHz,  $\text{DMSO-}d_6$ )  $\delta$  162.76, 161.77, 153.58, 150.63, 145.91, 143.80, 139.50, 130.63, 125.92, 124.50, 113.93, 97.33, 92.49, 55.98, 25.12, 23.09, 18.51, 10.60. HRMS (ESI):  $m/z$  calcd for  $\text{C}_{18}\text{H}_{18}\text{N}_9\text{S}$  ( $\text{M} + \text{H}$ ) $^+$ , 392.1406; found, 392.1402.

**Cell Culture.** The human colon cancer cell line SW620 and its MDR cell line, SW620/Ad300, were kindly supplied by Dr. Susan Bates's lab (NIH, MD). The ABCB1-overexpressed KB-C2 cell line was established by a step-wise exposure of KB-3-1 cells, a parental human epidermoid carcinoma cell line, to increasing concentrations (up to 2  $\mu\text{g}/\text{mL}$ ) of colchicine.<sup>47,48</sup> The human primary embryonic kidney cell line HEK293's ABCB1 stable gene-transfected cell line HEK293/ABCB1 and HEK293/pcDNA3.1 were obtained by trans-

fecting the HEK293 cells with ABCB1 expression vector or empty vector and were cultured in a medium with puromycin (1  $\mu\text{g}/\text{mL}$ ). All cell lines were maintained in the Dulbecco's modified Eagle's medium (DMEM), containing 10% fetal bovine serum and 1% penicillin and streptomycin at 37 °C with 5%  $\text{CO}_2$ .

**MTT Assay.** The MTT assay was performed to detect the sensitivity of cells to anticancer drugs *in vitro*.<sup>49</sup> Briefly, 3000 cells were seeded in each well of a 96-well plate. After attachment to the bottom of the well, cells were preincubated with or without the reversal agents (100  $\mu\text{L}/\text{well}$ ) for 4 h, and then different concentrations of paclitaxel were added into designated wells. After 72 h of incubation, 20  $\mu\text{L}$  of MTT solution (5  $\text{mg}/\text{mL}$ ) was added to each well for cell staining. After 4 h, the medium was removed and 150  $\mu\text{L}$  of DMSO was added to each well. Finally, the absorbance was determined at 570 nm using an ELx 800 Universal microplate reader (Bio-Tek, Inc.).  $\text{IC}_{50}$  was calculated using SPSS software. The data were shown as the mean  $\pm$  SD was obtained by three dependent experiments.

**Docking Analysis.** To investigate the interaction modes between compounds and human ABCB1, molecular docking studies were conducted using the AutoDock Tools package (version 1.5.6).<sup>50</sup> The model of human ABCB1 was obtained from homology modeling on the SWISS-MODEL server.<sup>51</sup> The apo form of mouse ABCB1 in the inward-open conformation (PDB code: 4Q9H), which could bind to a series of cyclic peptides such as QZ-Ala (PDB code: 4Q9I), QZ-Val (4Q9J), QZ-Leu (4Q9K), and QZ-Phe (4Q9L),<sup>40</sup> was used as the template for human ABCB1 modeling. In the docking simulation, **WS-36** and **WS-691** were used as ligands, while the human ABCB1 model was used as the receptor. The structures of ABCB1 and compounds were optimized and prepared to the pdbqt format files used for docking by AutoDock tools. For the human ABCB1 model, five grids files with varying xyz coordinates (70.95/−4.65/−9.74, 48.43/1.88/1.32, 76.87/13.42/5.17, 40.68/7.98/17.71, and 75.17/29.6/27.6) were generated to probe the whole structure of ABCB1, except for two ATPase domains. The dimensions of the docking grid were 20 Å  $\times$  20 Å  $\times$  20 Å. All of the other parameters were set to the default values. After this, **WS-36** and **WS-691** were docked to the receptor human ABCB1 model with 20 complexes output per docking run, and the results were ranked based on the value of their binding energies. The most minimal energy complex for each compound was then selected as the reliable binding mode. All results were analyzed and visualized using PyMOL (<http://www.pymol.org>).

**Western Blotting.** Cells were lysed on the ice for 30 min in RIPA buffer (Beyotime Biotechnology, Shanghai, China) with complete protease inhibitors (Biotool, Houston, TX). After centrifugation, the samples were loaded onto sodium dodecyl sulfate polyacrylamide gel electrophoresis (SDS-PAGE) and electrophoretically transferred onto poly(vinylidene fluoride) (PVDF) membranes. The membranes were blocked by 5% bovine serum albumin (BSA) in TBST and then incubated with the primary antibody at 4 °C overnight. The next day, the membranes were incubated with secondary antibody for 2 h at room temperature. The protein–antibody complex was detected by enhanced chemiluminescence.

**Immunofluorescence Assay.** Around 5000 cells were planted on the coverslip in the 24-well plate and incubated with **WS-691** at 20  $\mu\text{M}$  for 72 h. The cells were fixed by 4% formaldehyde, permeabilized by 0.1% Triton X-100, and blocked with 5% bull serum albumin before being incubated with primary antibody at 4 °C overnight. After rinsing, the cells were incubated with Alexa Fluor 488 rabbit anti-goat IgG for 2 h and Hoechst 33342. A laser scanning confocal microscope (Nikon A1R, Tokyo, Japan) was used to collect fluorescence images.<sup>52</sup>

**UPLC.** The intracellular concentration of paclitaxel was detected by ultra-performance liquid chromatography (UPLC).<sup>32</sup> Then, 5  $\times$  10<sup>6</sup> SW620/Ad300 cells were cultured in the medium in the presence or absence of **WS-691** (10 and 20  $\mu\text{M}$ ) or verapamil (4  $\mu\text{M}$ ) for 72 h. Then, the medium was replaced with fresh medium with 20  $\mu\text{M}$  PTX for another 3 h incubation. Subsequently, the cells were washed with cold phosphate-buffered saline (PBS) and resuspended in 1 mL of PBS. The cells were lysed by sonication and paclitaxel was extracted

with ethyl acetate. The standard curve was established using paclitaxel standard samples at a concentration range of 31–8000 ng/mL by UPLC. The retention time was 1.56 min. Finally, the concentration of intracellular PTX was calculated by a standard curve of UPLC.

**[<sup>3</sup>H]-PTX Accumulation and Efflux Assay.** The accumulation assay was performed as previously described.<sup>53</sup> The accumulation of [<sup>3</sup>H]-PTX in SW620 and SW620/Ad300 was detected in the presence or absence of verapamil or WS-691. The cells were incubated with WS-691 at 20 μM at or VPM at 4 μM, respectively, for 4 h at 37 °C, followed by the addition of 0.1 μM [<sup>3</sup>H]-PTX for another 2 h, which was then lysed and placed in 5 mL of scintillation liquid after washing with cold PBS three times. The Packard TRICARB 1900CA liquid scintillation analyzer (Packard Instrument, Downers Grove, IL) was used to detect the radioactivity. As for the [<sup>3</sup>H]-PTX efflux assay, after the addition of 0.1 μM [<sup>3</sup>H]-PTX for 2 h, the cells were incubated in the [<sup>3</sup>H]-free medium for another 2 h, during which each radioactivity data were collected at 0, 30, 60, and 120 min, respectively.

**ATPase Assay.** The ATPase assay was performed as previously described.<sup>54</sup> ABCB1 crude membrane vesicles were purchased from BD Biosciences (San Jose, CA), and 10 μg of membrane was incubated with or without sodium orthovanadate (0.3 mM) in assay buffer for 3 min. After that, 0–40 μM varying concentration of WS-691 was added to the assay buffer, respectively. The reaction was initiated upon adding 5 mM of Mg-ATP, followed by incubation at 37 °C for 20 min, and then was terminated by adding 100 μL 5% SDS solution. The ATPase activity due to ABCB1 was determined from the amount of inorganic phosphate (Pi) released detected at 880 nm using a spectrophotometer.

**Cellular Thermal Shift Assay (CETSA).** Typically, SW620/Ad300 cells (approximately  $3.2 \times 10^7$ ) were collected, washed, and then resuspended with PBS. The cell suspensions were freeze-thawed five times using liquid nitrogen. The lysate was separated by centrifugation at 15 000g for 20 min at 4 °C. The cell lysates were divided into two aliquots, with one aliquot being treated with WS-691 (200 μM) and the other aliquot with an equal amount of DMSO (1%, v/v). After 30 min incubation at room temperature, the respective lysates were divided into nine aliquots and heated individually at different temperatures for 3 min. The heated lysates were centrifuged at 20 000g for 20 min at 4 °C. The supernatants were transferred to new microtubes and analyzed by Western blotting analysis.

**CYP3A4 Assay.** The cytochrome P4503A4 (CYP3A4) activity assay was performed to study the effect of WS-691 and VPM on CYP3A4, exactly according to the instruction of the kit (Catalog # K701, Biovision). Ketoconazole was used as a positive CYP3A4 inhibitor control. Briefly, the compound (Ketoconazole, WS-691, or VPM), P450 Reaction Mix and CYP3A4 Assay Buffer were mixed and incubated for 10 min. The reaction was started by adding the CYP3A4 substrate/NADP<sup>+</sup>, and the fluorescence was immediately measured every 2 minutes at Ex/Em = 531/595 nm in kinetic mode at 37 °C.

**Xenograft Studies.** Animals were treated according to protocols established by the ethics committee of Zhengzhou University, and the *in vivo* experiments were carried out in accordance with the approved guidelines and approved by the ethics committee of Zhengzhou University. Briefly, male BALB/c nude mice (15–17 g, aged 5–6 weeks, Hunan SJA Laboratory Animal Co., Ltd, Hunan, China) were housed in individually ventilated cages and maintained with food and sterile water. Approximately  $8 \times 10^6$  SW620/Ad300 cells were inoculated subcutaneously into the right forelimb of each mouse. The mice were randomized into five groups ( $n = 6$ ) and treated with one of the following regimens: (i) vehicle (containing 90% corn oil, 5% castor oil, and 5% DMSO, 10 mL/kg/day, i.g.); (ii) PTX (5 mg/kg/3 days, i.v.); (iii) WS-691 (20 mg/kg/day, i.g.); (iv) PTX plus VPM hydrochloride (6 mg/kg/day, i.g.); (v) PTX plus WS-691. Following 21-day treatment, animals were euthanized by carbon dioxide, and tumor and liver tissue were fixed in 4% paraformaldehyde for immunohistochemistry.

**HE Staining.** Histopathology analysis was performed using HE staining. Briefly, tissue sections were deparaffinized and stained by Hematoxylin before being rinsed and differentiated by 1% hydro-

chloric acid in alcohol (v/v). Then, the sections were stained in Eosin solution. After being rinsed and paraffined, the slides were mounted in neutral balsam.

**TUNEL Assay.** TUNEL staining was performed according to the manufacturer's instructions (Dalian Meilun Biotechnology, Dalian, China). Briefly, tumor tissue sections were incubated with proteinase K (20 μg/mL) for 20 min at RT, then were rinsed with PBS. The sections were subsequently incubated with a buffer containing TdT enzyme and FITC-12-dUTP for 1 h at 37 °C in the dark conditions. The sections were sealed with antifluorescence attenuation sealant and the fluorescence of positive staining was examined using a fluorescence microscope.

**Statistical Analysis.** All experiments were repeated at least three times, and the differences were determined using the two-tailed Student's *t*-test and statistical significance was determined at  $P < 0.05$ .

## ■ ASSOCIATED CONTENT

### Supporting Information

The Supporting Information is available free of charge at <https://pubs.acs.org/doi/10.1021/acs.jmedchem.0c01741>.

Cell survival rates under the nontoxic concentration of compounds toward selected cancer cells NMR, HRMS, and HPLC spectra of compounds 5–55 (PDF)

Coordinates of modeled structures in PDB format: WS-36 in complex with ABCB1 (PDB code: 4Q9H) (PDB)

Coordinates of modeled structures in PDB format: WS-691 in complex with ABCB1 (PDB code: 4Q9H) (PDB)

Molecular formula strings (CSV)

## ■ AUTHOR INFORMATION

### Corresponding Authors

**Bin Yu** – School of Pharmaceutical Sciences & Key Laboratory of Advanced Drug Preparation Technologies, Ministry of Education, Zhengzhou University, Zhengzhou 450001, China; [orcid.org/0000-0002-7207-643X](https://orcid.org/0000-0002-7207-643X); Phone: +86-0371-67781908; Email: [yubin@zzu.edu.cn](mailto:yubin@zzu.edu.cn); Fax: +86-0371-67781908

**Zhe-Sheng Chen** – College of Pharmacy and Health Sciences, St. John's University, Queens, New York 11439, United States; [orcid.org/0000-0002-8289-097X](https://orcid.org/0000-0002-8289-097X); Phone: +1-718-990-1432; Email: [chenz@stjohns.edu](mailto:chenz@stjohns.edu); Fax: +1-718-990-1877

**Hong-Min Liu** – School of Pharmaceutical Sciences & Key Laboratory of Advanced Drug Preparation Technologies, Ministry of Education, Zhengzhou University, Zhengzhou 450001, China; [orcid.org/0000-0001-6771-9421](https://orcid.org/0000-0001-6771-9421); Phone: +86-0371-67781908; Email: [liuhm@zzu.edu.cn](mailto:liuhm@zzu.edu.cn); Fax: +86-0371-67781908

### Authors

**Shuai Wang** – School of Pharmaceutical Sciences & Key Laboratory of Advanced Drug Preparation Technologies, Ministry of Education, Zhengzhou University, Zhengzhou 450001, China

**Sai-Qi Wang** – Department of Oncology, The Affiliated Cancer Hospital of Zhengzhou University, Henan Cancer Hospital, Henan Cancer Institute, Zhengzhou 450008, China

**Qiu-Xu Teng** – College of Pharmacy and Health Sciences, St. John's University, Queens, New York 11439, United States

**Linlin Yang** – Department of Pharmacology, School of Basic Medical Sciences, Zhengzhou University, Zhengzhou 450001, China

Zi-Ning Lei – College of Pharmacy and Health Sciences, St. John's University, Queens, New York 11439, United States

Xiao-Han Yuan – School of Pharmaceutical Sciences & Key Laboratory of Advanced Drug Preparation Technologies, Ministry of Education, Zhengzhou University, Zhengzhou 450001, China

Jun-Feng Huo – School of Pharmaceutical Sciences & Key Laboratory of Advanced Drug Preparation Technologies, Ministry of Education, Zhengzhou University, Zhengzhou 450001, China

Xiao-Bing Chen – Department of Oncology, The Affiliated Cancer Hospital of Zhengzhou University, Henan Cancer Hospital, Henan Cancer Institute, Zhengzhou 450008, China

Mengru Wang – Department of Pharmacology, School of Basic Medical Sciences, Zhengzhou University, Zhengzhou 450001, China

Complete contact information is available at:

<https://pubs.acs.org/10.1021/acs.jmedchem.0c01741>

### Author Contributions

<sup>1</sup>S.W., S.-Q.W., Q.-X.T., and L.Y. contributed equally to this work.

### Notes

The authors declare no competing financial interest.

### ACKNOWLEDGMENTS

We would like to acknowledge financial support from the National Natural Science Foundation of China (Nos. 81773562, 81973177, and 81703326), the Program for Science & Technology Innovation Talents in Universities of Henan Province (No. 21HASTIT045), the China Postdoctoral Science Foundation (Nos. 2018M630840, and 2019T120641), Medical Science and Technique Foundation of Henan Province (Nos. 2018020486 and SB201901101), the Science and Technique Foundation of Henan Province (No. 202102310413), and 1000 Talents Program of Central plains (No. 204200510023). We appreciate Drs. Susan E. Bates and Robert Robey for the SW620 and SW620/Ad300 cell lines used in the study (NIH, Bethesda, MD). We thank Dr. Shin-Ichi Akiyama for KB-3-1 and KB-C2 cell lines (Kagoshima University, Kagoshima, Japan). Besides, we are thankful to Dr. Tanaji T. Talele (St. John's University, New York, NY) for providing the computing resources for docking analysis.

### ABBREVIATIONS USED

ABC, ATP-binding Cassette; ABCB1, MDR1, or P-glycoprotein, ATP-binding cassette subfamily B member 1; ATP, adenosine triphosphate; NBDs, nucleotide-binding domains; TMDs, transmembrane domains; MDR, multidrug resistance; ATP, adenosine triphosphate; CYP3A4, cytochrome P3A4; PTX, paclitaxel; RF, reversal fold; VPM, verapamil; SARs, structure–activity relationships; IFD, induce-fit docking; XP, the Glide extra precision; CETSA, cellular thermal shift assay; Cpd., compound; TLC, thin-layer chromatography; ESI, electrospray ionization; HPLC, high-performance liquid chromatography; NIH, National Institutes of Health; MTT, 3-(4,5-dimethylthiazol-2-yl)-2,5-diphenyltetrazolium bromide; DMEM, Dulbecco's modified Eagle's medium; PDB, protein data bank; SDS-PAGE, sodium dodecyl sulfate polyacrylamide gel electrophoresis; BSA, bovine serum albumin; PVDF, electrophoretically transferred onto polyvinylidene fluoride; HRP, horseradish peroxidase; UPLC, ultra-performance liquid

chromatography; PBS, phosphate-buffered saline; Pi, inorganic phosphate; DMSO, dimethyl sulfoxide; i.v., intravenous injection; i.g., intragastrical injection; RT, room temperature

### REFERENCES

- (1) Gottesman, M. M. Mechanisms of cancer drug resistance. *Annu. Rev. Med.* **2002**, *53*, 615–627.
- (2) Perez, R. P.; Hamilton, T. C.; Ozols, R. F.; Young, R. C. Mechanisms and modulation of resistance to chemotherapy in ovarian cancer. *Cancer* **1993**, *71*, 1571–1580.
- (3) Niewerth, D.; Jansen, G.; Assaraf, Y. G.; Zweegman, S.; Kaspers, G. J. L.; Cloosa, J. Molecular basis of resistance to proteasome inhibitors in hematological malignancies. *Drug Resist. Updates* **2015**, *18*, 18–35.
- (4) Fletcher, J. I.; Williams, R. T.; Henderson, M. J.; Norris, M. D.; Haber, M. ABC transporters as mediators of drug resistance and contributors to cancer cell biology. *Drug Resist. Updates* **2016**, *26*, 1–9.
- (5) Li, W.; Zhang, H.; Assaraf, Y. G.; Zhao, K.; Xu, X.; Xie, J.; Yang, D.-H.; Cheng, Z.-S. Overcoming ABC transporter-mediated multidrug resistance: molecular mechanisms and novel therapeutic drug strategies. *Drug Resist. Updates* **2016**, *27*, 14–29.
- (6) Gacche, R. N.; Assaraf, Y. G. Redundant angiogenic signaling and tumor drug resistance. *Drug Resist. Updates* **2018**, *36*, 47–76.
- (7) Assaraf, Y. G.; Brozovic, A.; Gonçalves, A. C.; Jurkovicovag, D.; Linē, A.; Machuqueiro, M.; Saponara, S.; Sarmiento-Ribeiro, A. B.; Xavier, C. P. R.; Vasconcelos, M. H. The multi-factorial nature of clinical multidrug resistance in cancer. *Drug Resist. Updates* **2019**, *46*, 100645–100675.
- (8) Dong, J.; Qin, Z.; Zhang, W.-D.; Cheng, G.; Yehuda, A. G., Jr; C, R. A.; Chen, Z.-S.; Cheng, X.-D.; Qin, J.-J. Medicinal chemistry strategies to discover P-glycoprotein inhibitors: An update. *Drug Resist. Updates* **2020**, *49*, 100681–100705.
- (9) Gottesman, M. M.; Fojo, T.; Bates, S. E. Multidrug resistance in cancer: role of atp-dependent transporters. *Nat. Rev. Cancer* **2002**, *2*, 48–58.
- (10) Chen, T.; Wang, C.; Liu, Q.; Meng, Q.; Sun, H.; Huo, X.; Sun, P.; Peng, J.; Liu, Z.; Yang, X.; Liu, K. Dasatinib reverses the multidrug resistance of breast cancer MCF-7 cells to doxorubicin by down-regulating P-gp expression via inhibiting the activation of ERK signaling pathway. *Cancer Biol. Ther.* **2015**, *16*, 106–114.
- (11) Baumert, C.; Hilgeroth, A. Recent advances in the development of P-gp inhibitors. *Anti-Cancer Agents Med. Chem.* **2009**, *9*, 415–436.
- (12) Szakács, G.; Varadi, A.; Ozvegy-Laczka, C.; Sarkadi, B. The role of ABC transporters in drug absorption, distribution, metabolism, excretion and toxicity (ADME-Tox). *Drug Discov. Today* **2008**, *13*, 379–393.
- (13) Binkhathlan, Z.; Lavasanifar, A. P-glycoprotein inhibition as a therapeutic approach for overcoming multidrug resistance in cancer: current status and future perspectives. *Curr. Cancer Drug Targets* **2013**, *13*, 326–346.
- (14) Tsuruo, T.; Iida, H.; Tsukagoshi, S.; Sakurai, Y. Overcoming of vincristine resistance in P388 leukemia in vivo and in vitro through enhanced cytotoxicity of vincristine and vinblastine by verapamil. *Cancer Res.* **1981**, *41*, 1967–1972.
- (15) Kelly, R. J.; Draper, D.; Chen, C. C.; Robey, R. W.; Figg, W. D.; Piekarz, R. L.; Chen, X.; Gardner, E. R.; Balis, F. M.; Venkatesan, A. M.; Steinberg, S. M.; Fojo, T.; Bates, S. E. A pharmacodynamic study of docetaxel in combination with the P-glycoprotein antagonist tariquidar (XR9576) in patients with lung, ovarian, and cervical cancer. *Clin. Cancer Res.* **2011**, *17*, 569–580.
- (16) Pennock, G. D.; Dalton, W. S.; Roeske, W. R.; Appleton, C. P.; Mosley, K.; Plezia, P.; Miller, T. P.; Salmon, S. E. Systemic toxic effects associated with high-dose verapamil infusion and chemotherapy administration. *J. Natl. Cancer Inst.* **1991**, *83*, 105–110.
- (17) Thomas, H.; Coley, H. M. Overcoming multidrug resistance in cancer: an update on the clinical strategy of inhibiting P-glycoprotein. *Cancer Control* **2003**, *10*, 159–165.

- (18) Bechtel, L. K.; Haverstick, D. M.; Holstege, C. P. Verapamil toxicity dysregulates the phosphatidylinositol 3-kinase pathway. *Acad. Emerg. Med.* **2008**, *15*, 368–374.
- (19) Koski, A.; Raki, M.; Kanerva, A.; Nokisalmi, P.; Pesonen, S.; Liikanen, I.; Kangasniemi, L.; Joensuu, T.; Alemany, R.; Hemminki, A. Verapamil results in increased blood levels of oncolytic adenovirus in treatment of patients with advanced cancer. *Mol. Ther.* **2012**, *20*, 221–229.
- (20) Wilson, W. H.; Jamis-Dow, C.; Bryant, G.; Balis, F. M.; Klecker, R. W.; Bates, S. E.; Chabner, B. A.; Steinberg, S. M.; Kohler, D. R.; Wittes, R. E. Phase I and pharmacokinetic study of the multidrug resistance modulator dexverapamil with EPOCH chemotherapy. *J. Clin. Oncol.* **1995**, *13*, 1985–1994.
- (21) Tidefelt, U.; Liliemark, J.; Gruber, A.; Liliemark, E.; Sundman-Engberg, B.; Juliusson, G.; Stenke, L.; Elmhorn-Rosenborg, A.; Möllgård, L.; Lehman, S.; Xu, D.; Covelli, A.; Gustavsson, B.; Paul, C. P-glycoprotein inhibitor valsopodar (PSC 833) increases the intracellular concentrations of daunorubicin in vivo in patients with P-glycoprotein-positive acute myeloid leukemia. *J. Clin. Oncol.* **2000**, *18*, 1837–1844.
- (22) Minderman, H.; Pendyala, L.; O'Loughlin, K. L.; Baer, M. R. VX-710 (Bircodan) Increases drug retention and enhances chemosensitivity in resistant cells overexpressing P-glycoprotein, multidrug resistance protein, and breast cancer resistance protein. *Clin. Cancer Res.* **2004**, *10*, 1826–1834.
- (23) Gottesman, M. M.; Ludwig, J.; Xia, D.; Szakacs, G. Defeating drug resistance in cancer. *Discovery Med.* **2009**, *6*, 18–23.
- (24) Kathawala, R. J.; Wang, Y. J.; Shukla, S.; Zhang, Y. K.; Alqahtani, S.; Kaddoumi, A.; Ambudkar, S. V.; Ashby, C. R., Jr.; Chen, Z. S. ATP-binding cassette subfamily B member 1 (ABCB1) and subfamily C member 10 (ABCC10) are not primary resistance factors for cabazitaxel. *Chin. J. Cancer* **2015**, *34*, No. 5.
- (25) LEONARD, G. D.; FOJO, T.; BATES, S. E. The Role of ABC Transporters in clinical practice. *Oncologist* **2003**, *8*, 411–424.
- (26) Szakacs, G.; Paterson, J. K.; Ludwig, J. A.; Booth-Genthe, C.; Gottesman, M. M. Targeting multidrug resistance in cancer. *Nat. Rev. Drug Discov.* **2006**, *5*, 219–234.
- (27) Shukla, S.; Wu, C.-P.; Ambudkar, S. V. Development of inhibitors of ATP-binding cassette drug transporters: present status and challenges. *Expert Opin. Drug Metab. Toxicol.* **2008**, *4*, 205–223.
- (28) Shukla, S.; Ohnuma, S.; Ambudkar, S. V. Improving cancer chemotherapy with modulators of ABC drug transporters. *Curr. Drug Targets* **2011**, *12*, 621–630.
- (29) Chen, Z.; Huang, C.; Shi, T.; Hu, T.; Zhang, L.; Jiang, L.; Li, J.; Zhu, P.; Deng, M. Mammalian drug efflux transporters of the ATP binding cassette (ABC) family in multidrug resistance: A review of the past decade. *Cancer Lett.* **2016**, *370*, 153–164.
- (30) Wang, B.; Ma, L.-Y.; Wang, J.-Q.; Lei, Z.-N.; Gupta, P.; Zhao, Y.-D.; Li, Z.-H.; Liu, Y.; Zhang, X.-H.; Li, Y.-N.; Zhao, B.; Chen, Z.-S.; Liu, H.-M. Discovery of 5-cyano-6-phenylpyrimidin derivatives containing an acylurea moiety as orally bioavailable reversal agents against P-glycoprotein-mediated multidrug resistance. *J. Med. Chem.* **2018**, *61*, 5988–6001.
- (31) Wang, B.; Zhao, B.; Chen, Z.-S.; Pang, L.-P.; Zhao, Y.-D.; Guo, Q.; Zhang, X.-H.; Liu, Y.; Liu, G.-Y.; Hao-Zhang; Zhang, X.-Y.; Ma, L.-Y.; Liu, H.-M. Exploration of 1,2,3-triazole-pyrimidine hybrids as potent reversal agents against ABCB1-mediated multidrug resistance. *Eur. J. Med. Chem.* **2018**, *143*, 1535–1542.
- (32) Chang, L.; Xiao, M.; Yang, L.; Wang, S.; Wang, S.-Q.; Bender, A.; Hui, A.; Chen, Z.-S.; Yu, B.; Liu, H.-M. Discovery of a non-toxic [1,2,4]triazolo[1,5-a]pyrimidin-7-one (WS-10) that modulates ABCB1-mediated multidrug resistance (MDR). *Bioorg. Med. Chem.* **2018**, *26*, 5006–5017.
- (33) Liu, Z.; Zhao, T.; Li, Z.; Sun, K.; Fu, Y.; Cheng, T.; Guo, J.; Yu, B.; Shi, X.; Liu, H. Discovery of [1,2,3]triazolo[4,5-d]pyrimidine derivatives as highly potent, selective, and cellularly active USP28 inhibitors. *Acta Pharm. Sin. B* **2020**, *10*, 1476–1491.
- (34) Wang, S.; Shen, D.; Zhao, L.; Yuan, X.; Cheng, J.; Yu, B.; Zheng, Y.; Liu, H. Discovery of [1,2,4]triazolo[1,5-a]pyrimidine derivatives as new bromodomain-containing protein 4 (BRD4) inhibitors. *Chin. Chem. Lett.* **2020**, *31*, 418–422.
- (35) Yuan, S.; Wang, S.; Zhao, M.; Zhang, D.; Chen, J.; Li, J.-X.; Zhang, J.; Song, Y.; Wang, J.; Yu, B.; Liu, H. Bronsted acid-promoted 'on-water' C(sp<sup>3</sup>)-H functionalization for the synthesis of isoindolinone/[1,2,4]triazolo[1,5-a]pyrimidine derivatives targeting the SKP2-CKS1 interaction. *Chin. Chem. Lett.* **2020**, *31*, 349–352.
- (36) Yuan, X.; Wang, S.; Cheng, J.; Yu, B.; Liu, H.-M. HFIP-promoted catalyst-free cascade reactions for the synthesis of biologically relevant 3,3-di(indolyl)indolin-2-ones from indoles and isatins. *Chin. Chem. Lett.* **2020**, *31*, 2465–2468.
- (37) Wang, S.; Zhao, L.; Shi, X.-J.; Ding, L.; Yang, L.; Wang, Z.-Z.; Shen, D.; Tang, K.; Li, X.-J.; Mamun, M. A. A.; Li, H.; Yu, B.; Zheng, Y.-C.; Wang, S.; Liu, H.-M. Development of highly potent, selective, and cellular active triazolo[1,5-a]pyrimidine-based inhibitors targeting the DCN1–UBC12 protein–protein interaction. *J. Med. Chem.* **2019**, *62*, 2772–2797.
- (38) Lu, N.; Huo, J.-l.; Wang, S.; Yuan, X.-H.; Liu, H.-M. Drug repurposing: Discovery of troxipide analogs as potent antitumor agents. *Eur. J. Med. Chem.* **2020**, *202*, No. 112471.
- (39) Wang, S.; Ma, X.-B.; Yuan, X.-H.; Yu, B.; Xu, Y.-C.; Liu, H.-M. Discovery of new [1,2,4]triazolo[1,5-a]pyrimidine derivatives that kill gastric cancer cells via the mitochondria pathway. *Eur. J. Med. Chem.* **2020**, *203*, No. 112630.
- (40) Szewczyk, P.; Tao, H.; McGrath, A. P.; Villaluz, M.; Rees, S. D.; Lee, S. C.; Doshi, R.; Urbatsch, I. L.; Zhang, Q.; Chang, G. Snapshots of ligand entry, malleable binding and induced helical movement in P-glycoprotein. *Acta Crystallogr., Sect. D: Biol. Crystallogr.* **2015**, *71*, 732–741.
- (41) Zhao, C.; Rakesh, K. P.; Ravidar, L.; Fang, W.-Y.; Qin, H.-L. Pharmaceutical and medicinal significance of sulfur (SVI)-containing motifs for drug discovery: A critical review. *Eur. J. Med. Chem.* **2019**, *162*, 679–734.
- (42) Silva, R.; Vilas-Boas, V.; Carmo, H.; Dinis-Oliveira, R. J.; Carvalho, F.; Bastos, M. d. L.; Remião, F. Modulation of P-glycoprotein efflux pump: induction and activation as a therapeutic strategy. *Pharmacol. Ther.* **2015**, *149*, 1–123.
- (43) Sharom, F. J.; Yu, X.; Chu, J. W. K.; Doige, C. A. Characterization of the ATPase activity of P-glycoprotein from multidrugresistant Chinese hamster ovary cells. *Biochem. J.* **1995**, *308*, 381–390.
- (44) Kathawala, R. J.; Gupta, P., Jr.; Ashby, C. R.; Chen, Z.-S. The modulation of ABC transporter-mediated multidrug resistance in cancer: A review of the past decade. *Drug Resist. Updates* **2015**, *18*, 1–17.
- (45) Boumendjel, A.; Baubichon-Cortay, H.; Trompier, D.; Perrotton, T.; Di Pietro, A. Anticancer multidrug resistance mediated by MRP1: Recent advances in the discovery of reversal agents. *Med. Res. Rev.* **2005**, *25*, 453–472.
- (46) Molina, D. M.; Jafari, R.; Ignatushchenko, M.; Seki, T.; Larsson, A.; Dan, C.; Sreekumar, L.; Cao, Y.; Nordlund, P. Monitoring drug target engagement in cells and tissues using the cellular thermal shift assay. *Science* **2013**, *341*, 84–87.
- (47) Akiyama, S.-i.; Fojo, A.; Hanover, J. A.; Pastan, I.; Gottesman, M. M. Isolation and genetic characterization of human KB cell lines resistant to multiple drugs. *Somatic Cell Mol. Genet.* **1985**, *11*, 117–126.
- (48) Akiyama, S.-i.; Setti, P.; Pirker, R.; FitzGerald, D.; Gottesman, M. M.; Pastan, I. Potentiation of cytotoxic activity of immunotoxins on cultured human cells. *Cancer Res.* **1985**, *45*, 1005–1007.
- (49) She, S.; Wu, X.; Zheng, D.; Pei, X.; Ma, J.; Sun, Y.; Zhou, J.; Nong, L.; Guo, C.; Lv, P.; Song, Q.; Zheng, C.; Liang, W.; Huang, S.; Li, Q.; Liu, Z.; Song, Z.; Li, Y.; Wang, Y.; et al. PSMF/MSMP promotes hepatic fibrosis through CCR2 and represents a novel therapeutic target. *J. Hepatol.* **2020**, *72*, 506–518.
- (50) Morris, G. M.; Huey, R.; Lindstrom, W.; Sanner, M. F.; Belew, R. K.; Goodsell, D. S.; Olson, A. J. AutoDock4 and autoDockTools4: Automated docking with selective receptor flexibility. *J. Comput. Chem.* **2009**, *30*, 2785–2791.

(51) Waterhouse, A.; Bertoni, M.; Bienert, S.; Studer, G.; Tauriello, G.; Gumienny, R.; Heer, F. T.; de Beer, T. A. P.; Rempfer, C.; Bordoli, L.; Lepore, R.; Schwede, T. SWISS-MODEL: homology modelling of protein structures and complexes. *Nucleic Acids Res.* **2018**, *46*, W296–W303.

(52) Wang, S. Q.; Wang, C.; Chang, L. M.; Zhou, K. R.; Wang, J. W.; Ke, Y.; Yang, D. X.; Shi, H. G.; Wang, R.; Shi, X. L.; Ma, L. Y.; Liu, H. M. Geridonin and paclitaxel act synergistically to inhibit the proliferation of gastric cancer cells through ROS-mediated regulation of the PTEN/PI3K/Akt pathway. *Oncotarget* **2016**, *7*, 72990–73002.

(53) Zhang, W.; Fan, Y. F.; Cai, C. Y.; Wang, J. Q.; Teng, Q. X.; Lei, Z. N.; Zeng, L.; Gupta, P.; Chen, Z. S. Olmutinib (BI1482694/HM61713), a novel epidermal growth factor receptor tyrosine kinase inhibitor, reverses ABCG2-mediated multidrug resistance in cancer cells. *Front. Pharmacol.* **2018**, *9*, 1097.

(54) Wang, J.-Q.; Li, J. Y.; Teng, Q.-X.; Lei, Z.-N.; Ji, N.; Cui, Q.; Zeng, L.; Pan, Y.; Yang, D.-H.; Chen, Z.-S. Venetoclax, a BCL-2 inhibitor, enhances the efficacy of chemotherapeutic agents in Wild-Type ABCG2-overexpression-mediated MDR cancer cells. *Cancers* **2020**, *12*, 466.